Journal Pre-proofs

Geochemistry of basaltic blueschists from the Deyader Metamorphic Complex (Makran Accretionary Prism, SE Iran): New constraints for magma generation in the Makran sector of the Neo-Tethys

Emilio Saccani, Morteza Delavari, Asghar Dolati, Luca Pandolfi, Edoardo Barbero, Renzo Tassinari, Michele Marroni

PII: S1367-9120(22)00064-5
DOI: https://doi.org/10.1016/j.jseaes.2022.105141
Reference: JAES 105141

To appear in: *Journal of Asian Earth Sciences*

Received Date: 2 December 2021
Revised Date: 26 January 2022
Accepted Date: 6 February 2022

Please cite this article as: Saccani, E., Delavari, M., Dolati, A., Pandolfi, L., Barbero, E., Tassinari, R., Marroni, M., Geochemistry of basaltic blueschists from the Deyader Metamorphic Complex (Makran Accretionary Prism, SE Iran): New constraints for magma generation in the Makran sector of the Neo-Tethys, *Journal of Asian Earth Sciences* (2022), doi: https://doi.org/10.1016/j.jseaes.2022.105141

Geochemistry of basaltic blueschists from the Deyader Metamorphic Complex (Makran Accretionary Prism, SE Iran): New constraints for magma generation in the Makran sector of the Neo-Tethys.

Emilio Saccani[1], Morteza Delavari[3], Asghar Dolati[3], Luca Pandolfi[4,5], Edoardo Barbero[1], Renzo Tassinari[1], Michele Marroni[4,5]

1 Dipartimento di Fisica e Scienze della Terra, Università di Ferrara, 44123 Ferrara, Italy; brbdrd@unife.it (E.B.); sac@unife.it (E.S.); tsr@unife.it (R.T.)

3 Faculty of Earth Sciences, Kharazmi University, Tehran 15719-19911, Iran; delavari@khu.ac.ir (M.D.); dolati@khu.ac.ir (A.D.)

4 Dipartimento di Scienze della Terra, Università di Pisa, 56126 Pisa, Italy; luca.pandolfi@unipi.it (L.P.); michele.marroni@unipi.it (M.M.)

5 Istituto di Geoscienze e Georisorse, Consiglio Nazionale delle Ricerche (CNR), 56124 Pisa, Italy

* Corresponding author: Emilio Saccani (sac@unife.it)

Abstract

The North Makran Domain in the Makran Accretionary Prism consists of an imbricate

stack of Mesozoic Neo-Tethyan ophiolitic and metaophiolitic units. The Deyader Complex is an important metamorphic unit of this Domain and includes tectonic slices of HP-LT blueschists derived from upper oceanic crust protoliths. The volcanic protoliths consist of basalts with Mg#=75.1-62.7, SiO_2 =41.59–48.02 wt%, and TiO_2 =0.79–1.53 wt%. Based on incompatible and REE contents and ratios, three geochemical types can be distinguished. Group 1 basalts show trace element compositions, and La_N/Yb_N and La_N/Sm_N ratios <1 resembling those of normal-type (N-) mid-ocean ridge basalts (MORB). Compared to N-MORBs, Group 2 basalts show slight enrichment in Th, Ta, Nb, as well as La_N/Yb_N and La_N/Sm_N ratios = ~1 similar to those observed in enriched-type (E-) MORB. Group 3 basalts show a transitional-alkaline nature (Nb/Y=0.7-1.0), marked Th, Ta, Nb enrichment and high La_N/Yb_N (4-7) and La_N/Sm_N (2–3.5) ratios resembling those of plume-type (P-) MORB. Trace element and REE petrogenetic models show that N-MORB protoliths were generated from a depleted MORB mantle source (DMM), whereas E-MORB and P-MORB protoliths were generated from partial melting of a DMM source that was metasomatized to variable extents by OIB-type chemical components. The Deyader blueschists protoliths show close geochemical and petrogenetic similarities with all the North Makran ophiolites, suggesting that they were formed in a large Late Jurassic – Cretaceous oceanic basin that was strongly affected by mantle plume activity and different extents of plume-ridge interaction.

Keywords: Ophiolite, Geochemistry, Petrology, Blueschist, Oceanic crust, Makran Accretionary Prism, Iran

1. Introduction

The Alpine-Himalayan belt is made up of several distinct orogenic belts, which are largely associated with the geodynamic evolution of distinct sectors and/or minor branches of the Tethyan Ocean and were formed by distinct episodes of subduction and continental collision that operated in different times and sectors from Permian to Cenozoic (e.g., Dercourt et al., 1986; Stampfli et al., 1991; Şengör, 1990; Dilek and Furnes, 2011). The Makran Accretionary Prism (SE Iran-SW Pakistan) represents the central segment of the Alpine-Himalayan belts, connecting the Zagros to the west and the Himalayas to the east (Fig. 1a), and its formation is associated with the Mesozoic geodynamic evolution of the Makran sector of the Neo-Tethys (McCall and Kidd 1982; Barrier et al., 2018). It represents a spectacular example of subduction-related accretionary prism (e.g., Kopp et al., 2000) and it is an outstanding natural laboratory for understanding the mechanisms of oceanic formation and the evolution of subduction zones. In the last two decades, increasing extensive research has been carried out in the Makran, particularly in the Cretaceous North Makran Domain (Figs. 1a, b) (e.g., Ghazi et al., 2004; Burg et al., 2008, 2013; Dolati, 2010; Dolati and Burg, 2013; Hunziker, 2014; Hunziker et al., 2015, 2017; Moslempour et al., 2015; Mohammadi et al., 2016; Dorani et al., 2017; Burg, 2018; Saccani et al., 2018; Esmaeili et al., 2020, 2021; Barbero et al., 2020a, 2020b, 2021a, 2021b; Barbero, 2021; Monsef et al., 2019; Pandolfi et al., 2021; Sepidbar et al., 2020). These studies have shown that the North Makran consists of an imbricate stack of tectonic units mainly including Cretaceous ophiolitic units, minor volcanic arc units, and a Coloured Mélange unit. Structural, petrological, biostratigraphic, and geochronological studies have shown that, in contrast to previous interpretations, the North Makran ophiolitic units largely consist of portions of Cretaceous oceanic crust and seamounts strongly influenced by mantle plume activity (Esmaeili et al., 2020; Barbero et al., 2020a;

Barbero et al., 2021a, 2021b). Recent detailed structural-geochronological studies have shown that the North Makran ophiolites are affected by different degrees of deformation ad metamorphism, which may characterize different ophiolitic units, but also different sequences within the same ophiolitic unit (Hunziker et al., 2017; Barbero et al., 2020b, 2021a, 2121b; Pandolfi et al., 2021).

Despite extensive research over the last decade, there are still some disparities in the level of knowledge of some ophiolitic and metaophiolitic units of the North Makran Domain. An example is represented by the high pressure - low temperature (HP-LT) metaophiolites of the Blueschist Unit in the Deyader Metamorphic Complex (Figs 1b, 2). Previous studies have excellently described the deformation and metamorphic evolution of this Unit but have only outlined the essential geochemistry and tectono-magmatic setting of formation of the magmatic protoliths (Hunziker, 2014; Hunziker et al., 2017). These studies were fundamental for reconstructing the tectonic mechanisms active during the Cretaceous subduction and closure of the Tethys Ocean, as well as during the early exhumation phases. However, in these studies the Deyader blueschists were basically interpreted as derived from mafic intrusive, extrusive, and volcaniclastic rocks representing fragments of oceanic crust. Nonetheless, it is commonly accepted that different geochemical features of ophiolites and metaophiolites are related to different mantle source characteristics and different petrogenetic processes, which are associated, in turn, with distinct tectono-magmatic settings of formation (e.g., Pearce, 2008; Dilek and Furnes, 2011; Saccani, 2015). Therefore, any interpretation of the pristine characteristics of the oceanic lithosphere in which ophiolitic or metaophiolitic sequences were formed must take account of the detailed geochemical, petrological, and tectono-magmatic characteristics of the ophiolitic magmatic rocks. In this paper we therefore present new whole rock geochemical data on Deyader blueschists derived from mafic volcanic protoliths with the aims of: a) defining the petrogenetic processes behind the

formation of the volcanic protoliths; b) providing robust constraints about the geochemical nature of the oceanic lithosphere in which they were formed. Unfortunately, the age of formation of the volcanic protoliths of the Deyader blueschists cannot be determined and, therefore, their tectono-magmatic significance within the Makran sector of the Neo-Tethys cannot be assessed in detail. Nonetheless, a geochemical comparison between the Deyader blueschists and other North Makran ophiolitic and metaophiolitic rocks will be carried out in order to evaluate their relationships with respect to other fragments of the same sector of the Neo-Tethys. A better definition of the nature of the oceanic lithosphere in which the Deyader blueschists were formed will be crucial in future regional scale reconstructions of the geodynamic evolution of the Makran Neo-Tethys.

2. Geological setting

2.1. General geological setting of the Makran Accretionary Prism

The Makran Accretionary Prism, which extends from SE Iran to SW Pakistan (Fig.1a), developed above the subduction zone resulting from the north-dipping subduction of the Neo-Tethys Ocean below the southern margin of Eurasia (McCall and Kidd, 1982; Dercourt et al., 1986; Saccani et al., 2018; Burg, 2018; Monsef et al., 2018; Barbero et al., 2020a, 2021a). The present-day deformation front of the accretionary prism is located offshore in the Oman Sea (McCall and Kidd 1982; Dercourt et al. 1986; Burg et al. 2008, 2013). The onshore Makran Accretionary Prism is bounded to the north by the Jaz Murian depression and is characterized by the tectonic juxtaposition of several tectono-stratigraphic domains (Dolati, 2010; Burg et al., 2013; Figs. 1a, b). These domains are from the structural top to the bottom

(from north to south): 1) the North Makran; 2) the Inner Makran; 3) the Outer Makran; 4) the Coastal Makran (Fig. 1a). The Inner, Outer, Coastal Makran Domains represent the post-Eocene accretionary complex. (e.g., Dolati, 2010; Dolati and Burg, 2013; Burg et al., 2013; Burg, 2018; Esmaeili et al., 2020). The North Makran Domain represents remnants of the pre-Eocene accretionary prism and consists of a tectonic stack of ophiolitic and volcanic arc units (Saccani et al., 2018; Esmaeili et al., 2020; Barbero et al., 2021b, Pandolfi et al., 2021). The ophiolitic rocks were interpreted as a remnant of the North Makran Ocean, a branch of the Neo-Tethys, which accreted to the Iranian microcontinent during Jurassic-Cretaceous times (Şengör 1990). The North Makran units include from the higher to the lowermost structural position (Fig. 1b): 1) the Ganj Complex; 2) the Northern Ophiolites; 3) the high pressure metamorphic Deyader Complex; 4) the Bajgan and Durkan Complexes; 5) the Sorkhband – Rudan tectonic slices; 6) the Coloured Mélange Complex. Some of these units show variable degrees of metamorphic imprint, ranging from low-grade greenschist facies condition in some sequences of the Durkan Complex (Barbero et al., 2021a, b) to blueschist facies condition in the Bajgan (McCall, 2002; Dorani et al., 2017, Pandolfi et al., 2021) and Deyader (Hunziker et al., 2017) Complexes.

The Ganj Complex represents fragments of a Late Cretaceous volcanic arc that was likely built up close to the southern margin of the Lut Block (Barbero et al., 2020a). The Northern Ophiolites are Early to Late Cretaceous in age and include the Band-e-Zeyarat/Dar Anar (Ghazi et al., 2004; Barbero et al., 2020b), Remeshk-Mokhtarabad (McCall, 2002; Hunziker et al., 2015; Burg, 2018), and Fannuj-Maskutan (Moslempour et al., 2015; Sepidbar et a., 2020) ophiolitic complexes. These ophiolites basically consist of cumulitic and isotropic gabbros, sheeted dykes, and volcanic sequences. In the Fannuj-Maskutan ophiolites upper mantle-lower crustal sequences have been reported (Hunziker, 2014). The Deyader Complex crops out in the eastern sector of the North Makran, and it is overthrust by the North Makran

ophiolites (Figs. 1b, 2). It consists of a low-grade metamorphic complex with metaophiolites that have experienced high pressure-low temperature (HP-LT) metamorphism (McCall, 2002; Hunziker et al., 2015, 2017). The scarce geochronological data indicate an age of about 89 Ma (K–Ar ages on sodic amphibole; Delaloye and Desmons, 1980). The Bajgan and Durkan Complexes were regarded as a Paleozoic metamorphic basement and its continental platform, respectively that were separated from the Lut Block in the Late Jurassic - Early Cretaceous. (e.g., McCall, 2002; Hunziker et al., 2015). However, recent data show that the Bajgan Complex mainly consists of metamorphosed incomplete ophiolitic sequences including cumulitic ultramafic and mafic rocks, isotropic gabbros, plagiogranites, and volcanic and volcaniclastic sequences (Pandolfi et al., 2021). Magmatic protoliths range in age from 161 to 114 Ma and have been affected by polyphase deformation that reached the blueschist metamorphic facies in the Late Cretaceous. Recent studies have shown that the Durkan Complex consists of volcano-sedimentary sequences representing a Late Cretaceous seamount chain incorporated as tectonic slices into the North Makran accretionary prism (Barbero et al., 2021a, 2021b). The Sorkhband and Rudan ophiolites crop out in the western part of the North Makran within the shear zone between the Coloured Mélange and the Bajgan Complex (McCall, 2002; Delavari et al., 2016). They largely consist of peridotites formed in a supra-subduction zone setting (Moghadam et al., 2022) The Coloured Mélange Complex is composed of metric- to decametric-thick tectonic slices and was formed in Cretaceous-Paleocene times (McCall and Kidd, 1982; McCall, 2002; Burg, 2018; Esmaeili et al., 2020). This mélange incorporates a great variety of volcanic and meta-volcanic rock-types formed in both the subducting oceanic plate and the upper plate (Saccani et al., 2018; Esmaeili et al., 2020, 2021).

2.2. Geological setting of the blueschists of the Deyader Metamorphic Complex

The geology, structural setting, and metamorphic evolution of the blueschist outcrops in the Deyader Complex have exhaustively been described by Hunziker et al. (2017); therefore, the following description will be essentially based on this work. The Deyader Metamorphic Complex crops out with faulted and thrust contacts with the Fannuj-Maskutan ophiolites (Fig. 2). It largely consists of dismembered and tectonically juxtaposed slices of very low- to low-grade metasedimentary rocks whose protoliths are represented by shales, sandstones, pebbly mudstones, and limestones (Hunziker, 2014). Blocks and outcrops of HP-LT metabasic rocks (blueschists) are subordinate in volume and mainly cluster in the NE corner of the Deyader Complex (Fig. 2). The largest blueschist outcrop forms a ~30 km^2–wide klippen onto the low-grade metasedimentary rocks and exposes a ~3 km-thick continuous section (see Hunziker et al., 2017 for a detailed description).

Blueschists were classified in the field based on their macroscopic texture into: 1) metapillow lavas; 2) fine-grained massive blueschists; 3) coarse-grained massive blueschists; 4) metavolcano-sedimentary sequences (layered blueschists of Hunziker et al., 2017). Metapillows show weak deformation and, therefore, the original pillow textures can be easily recognized in the field (Figs. 3a, b). Metapillow lavas are frequently associated with fine-grained marbles (Figs. 3a, b), which most likely represent original calcareous sediments deposited either as intra-pillow material, or as the pillow sedimentary cover. Fine-grained massive blueschists show grain size <0.5 mm and a weak foliation (Figs. 3c, d). They are found either in single slices and blocks or as thick (>1 m) layers within metavolcano-sedimentary (layered) blueschists. Due to their fine-grained, homogeneous texture, they most likely represent basaltic protoliths erupted as massive lava flows (see also Hunziker et al., 2017). Coarse-grained massive blueschists show grain size >0.5 mm and foliation marked by centimetric-thick compositional layering (Figs. 3e, e_1), which most likely represents an

original magmatic layering. For this reason, these rocks are interpreted as metagabbros. The metavolcano-sedimentary sequences mainly consist of alternations of thin (few cm) layers of metalavas and metasedimentary rocks, which frequently include thick (>1 m) metapillow lavas (Fig. 3f) or fine-grained massive blueschists. These metasedimentary rocks are shales showing very thin (few mm) foliation. P–T estimates of different blueschist protoliths yielded metamorphic peak conditions of 300–380°C at 0.9–1.4 GPa (Hunziker et al., 2017). These authors have demonstrated that the Deyader blueschists have experienced a four-stages metamorphic evolution, which defines a counterclockwise path: from early amphibolite facies metamorphism to amphibolite-blueschist transition, blueschist facies metamorphic peak, and finally a retrograde re-equilibration in the pumpellyite–actinolite facies.

3. Sampling and petrography

Since the scope of this paper is to study the petrogenetic processes that were responsible for the formation of the magmatic protoliths of the blueschists, sampling was focused on the fine-grained blueschist and metapillow lava varieties, which are thought to derive from volcanic protoliths. In fact, the compositions of the volcanic rocks most likely represent magmatic liquid compositions and can, therefore, reliably be used for petrogenetic studies (e.g., Pearce and Norry, 1979; Pearce, 2008; Saccani, 2015). In contrast, coarse-grained and metavolcano-sedimentary blueschists types were not studied in this paper as they most likely represent original gabbroic and volcaniclastic rocks, respectively (Hunziker et al., 2017) and, therefore, their compositions do not reliably represent “true” magmatic liquid compositions. Samples MK221, MK222, MK224, MK228, and MK229 show grano-porphyroblastic texture with porphyroblasts of large (up to 2 mm in length) hornblende surrounded by a fine-grained

aggregate (< 0.2 mm) of Na-amphibole, prismatic lawsonite crystals, pumpellyite and minor chlorite, as well as titanite as accessory phase (Figs. 4a, b). Na-amphibole is represented by glaucophane as testified by its typical lavender-blue colour and weak pleochroism, as well as distinctive negative elongation. This observation is in agreement with mineral chemical data shown by Hunziker et al., 2017). The small crystals of amphibole, lawsonite, and pumpellyite commonly show a granoblastic texture (Fig. 4b). Nonetheless, these minerals locally display a weak preferred orientation defining a lepidoblastic texture that wraps around large hornblende porphyroblasts. In samples MK221 and MK222, some layers of relatively bigger (~0.5 mm) crystals of glaucophane + lawsonite showing nematoblastic texture can be observed. Though titanite is an accessory phase, it is relatively abundant and locally shows coarse-grained, lozenge-shaped crystals oriented parallel to the foliation (Fig. 4a). Porphyroblasts likely represent relicts of magmatic pyroxene phenocrysts that have been pseudomorphosed by metamorphic amphiboles.

Samples MK223, MK226, MK227, and MK230 are characterized by a well-defined nematoblastic texture marked by prismatic and elongated hornblende, glaucophane, and lawsonite together with minor quartz with undulatory extinction and accessory titanite, apatite and rutile (Figs. 4c, d). Sample MK226 also contains accessory allanite as anhedral, very fine-grained (<0.05 mm) crystals (Fig. 4d). Hornblende occurs as relatively large crystals (0.5 – 1 mm) and show pleochroism ranging from pale yellow to green. Prismatic lawsonite is subordinate in volume compared to amphibole and usually shows comparatively smaller crystals ranging in size from 0.2 to 0.5 mm.

Sample MK225 shows a very fine-grained texture and a well-developed foliation defined by the preferential orientation of elongated crystals of glaucophane (pleochroism from colourless to light blue), hornblende (pleochroism from pale yellow, pale green to green), and anhedral titanite (Figs. 4e, f). Prismatic lawsonite with equant shape and very small epidote

crystals are broadly oriented along the foliation (Fig. 4f). This foliation is gently folded at the microscale by open to gentle folds (Fig. 4e).

A common feature of all the studied samples is the replacement of the outermost rims of the hornblende by glaucophane, which can be seen in either the larger porphyroblasts (Fig. 4a) or in the smallest crystals, as well (Fig. 4f). In addition, large hornblende porphyroblasts often show replacement by glaucophane also along intra-crystal fractures and cracks (Figs. 4a, d). Finally, glaucophane shows no later overprint. These features have also been described by Hunziker et al. (2017). According to these authors, this evidence suggests that an early amphibolite facies has been preserved. In addition, the coexistence of epidote and lawsonite suggests that also epidote was most likely preserved from an early stage of medium temperature-medium pressure metamorphism.

4. Analytical methods

Whole rock major and some trace elements were analysed by X-ray fluorescence (XRF) on pressed-powder pellets, using an ARL Advant-XP automated X-ray spectrometer. The matrix correction method proposed by Lachance and Trail (1966) was applied. Volatile contents were determined as loss on ignition (L.O.I.) at 1000°C. For the discussion of the geochemical characteristics of the studied rocks, major element composition has been re-calculated on L.O.I.-free bases. The rare earth elements (REE) and some trace elements (Rb, Sr, Zr, Y, Nb, Hf, Ta, Th, U) were determined by inductively coupled plasma-mass spectrometry (ICP-MS) using a Thermo Series X-I spectrometer. All whole rock analyses were performed at the Department of Physics and Earth Sciences of the Ferrara University; results are shown in Table 1. The accuracy of the XRF and ICP-MS data were evaluated using

results for international standard rocks run as unknown. The detection limits for XRF and ICP-MS analyses were evaluated using results from several runs of twenty-nine international standards. Results are the same as those reported in Barbero et al. (2021b) and are given in Supplementary Table S1.

5. Whole rock geochemistry

We describe the geochemical features of the Deyader blueschists using those elements that are virtually immobile during alteration and metamorphism. They include some incompatible trace elements (e.g., Ti, P, Zr, Y, Sc, Nb, Ta, Hf, Th), and REE, as well as some transition metals (e.g., Ni, Co, Cr, V). Large ion lithophile elements (LILE) and most major elements are commonly mobilized during alteration (Pearce and Norry, 1979).

No systematic chemical differences can be observed between the metapillow lavas and the fine-grained massive blueschists (Table 1); therefore, we describe these rocks collectively in this section. The protoliths of the studied blueschists are represented by basalts (Fig. 5) with Mg# values ranging from 75.1 to 62.7 suggesting that these basalts likely represent melts at a low degree of magmatic fractionation. All samples show similar contents of major elements and many trace elements (e.g., SiO_2, = 41.59 – 48.02 wt%, TiO_2 = 0.79 – 1.53 wt%, Al_2O_3 = 12.34 – 15.68 wt%, MgO = 9.38 – 14.62 wt%, CaO = 6.52 – 11.78 wt%, Ga = 10 – 19 ppm, Zn = 68 – 98 ppm, Sc = 23 – 38 ppm, V = 202 – 356 ppm, Ni = 78 – 189 ppm, Cr = 271 – 460 ppm, see Table 1). The relatively high contents of MgO and Cr also testify for a rather primitive nature of the basaltic protoliths. On the other hand, some incompatible elements (including REE), as well as some elemental ratios show a wide range of variation. In

fact, based on incompatible elements and REE compositions, three geochemical types can be distinguished (hereafter Group 1, Group 2, and Group 3).

5.1. Group 1 basaltic protoliths

Group 1 metabasalts display a sub-alkaline nature with relatively low Nb/Y ratio (0.09 – 0.13, Fig. 5) and are characterized by generally low abundance of Y (20.1 – 29.2 ppm), Zr (56.9 – 72 ppm), Nb (2.48 – 2.62 ppm), Th (0.136 – 0.185 ppm), U (0.058 – 0.076 ppm), and Ta (0.136 – 0.176 ppm), as well as low Nb/Yb (0.85 – 1.15), Ta/Yb (0.05 – 0.07), and Th/Yb (0.05 – 0.06) ratios (Table 1). In the N-MORB-normalized incompatible elements spider diagram (Fig. 6a), these rocks show rather flat patterns, with either slightly positive or slightly negative anomalies in Ti. Contents of LILE (e.g., Ba) and high field strength elements (HFSE; e.g., Hf, Zr, Y) are low, ranging from ~1.6 to 3 and from ~0.7 to 1 times N-MORB composition (Sun and McDonough, 1989), respectively. Chondrite-normalized REE patterns (Fig. 6b) are rather flat from MREE to HREE, whereas LREE show moderate depletion compared to MREE and HREE, as exemplified by the $(Sm/Yb)_N$ (0.94–1.02), $(La/Yb)_N$ (0.62–0.77) and $(La/Sm)_N$ (0.66–0.78) ratios (Fig. 7). MK229 is the only sample showing a slightly negative Eu anomaly (Fig. 6b). HREE contents are slightly lower than those of the typical N-MORB (Fig. 6b) with Yb_N values ranging from ~13 to 17 times Chondrite abundance (Sun and McDonough, 1989). The incompatible and REE compositions of Group 1 metabasalts are well comparable with those of typical N-MORBs (Figs. 6a, b). In the discrimination diagram in Figure 8, the Group 1 metabasalts plot close to the composition of N-MORBs (Saccani, 2015).

5.2. Group 2 basaltic protoliths

Group 2 metabasalts display a sub-alkaline nature with relatively low Nb/Y ratios (~0.15, Fig. 5). Though generally low, these ratios are slightly higher than those of the Group 1 metabasalts and overlap the Nb/Y values for E-MORBs from various ophiolitic units of the North Makran (Fig. 5). Likewise, though generally low, the abundances of Y (27.2 – 29.0 ppm), Zr (81.4 – 95 ppm), Nb (3.98 – 4.42 ppm), Th (0.346 – 0.407 ppm), U (0.133 – 0.164 ppm), and Ta (0.248 – 0.272 ppm), as well as Nb/Yb (1.40 – 1.43), Ta/Yb (0.09), and Th/Yb (0.12 – 0.13) ratios are comparatively higher than those of Group 1 metabasalts (Table 1). In the N-MORB-normalized incompatible elements spider diagram (Fig. 6c), Group 2 metabasalts show patterns slightly decreasing from Th to Yb with LILE ranging from ~4 to ~7 times N-MORB composition and HFSE around 1 time N-MORB composition (Sun and McDonough, 1989). REE show very flat Chondrite-normalized patterns (Fig. 6d), as exemplified by $(Sm/Yb)_N$, $(La/Yb)_N$, and $(La/Sm)_N$ ratios around 1 (Fig. 7). HREE contents are similar to those of the typical N-MORB with Yb_N values ranging from ~16 to 19 times Chondrite abundance (Sun and McDonough, 1989). The incompatible and REE compositions of Group 2 metabasalts show similarities with either E-MORB or oceanic plateau basalt (OPB) compositions (Figs. 6c, d). In the discrimination diagram in Figure 8, the Group 2 metabasalts plot between the compositions of N- and E-MORBs (Saccani, 2015) and overlap the compositions of both E-MORB and OPB rocks from various ophiolitic units of the North Makran.

5.3. Group 3 basaltic protoliths

Group 3 metabasalts display a transitional-alkaline nature with relatively high Nb/Y ratio (0.64 – 0.78, Fig. 5) and are characterized by moderately high abundance of Y (22.0 – 33.5

ppm) and Zr (97.0 – 124 ppm), and high abundance of Nb (17.2 – 25.1 ppm), Th (1.51 – 2.35 ppm), U (0.460 – 0.691 ppm), and Ta (1.11 – 1.59 ppm), as well as high Ta/Yb (0.45 – 0.62), and Th/Yb (0.61 – 0.83) ratios and very high Nb/Yb (7.15 – 8.85) ratios (Table 1). In the N-MORB-normalized incompatible elements spider diagram (Fig. 6c), these rocks show patterns regularly and steeply decreasing from N-MORB normalized values for Th to Yb. Th, Ta, and Nb are approximately in the range 7 – 20, whereas Yb_N is in the range 0.6 – 0.9 times N-MORB composition (Sun and McDonough, 1989). Chondrite-normalized REE patterns (Fig. 6d) are characterized by significant enrichment in LREE compared to MREE and HREE, as exemplified by the $(La/Yb)_N$ (3.85–7.02) and $(La/Sm)_N$ (1.96 – 3.49) coupled with slight MREE/HREE enrichment (Sm_N/Yb_N = 1.85–2.01). These REE features are well summarized in Figure 7. HREE contents are slightly lower than those of the typical N-MORB (Yb_N = 17.9, Fig. 6d) with Yb_N values ranging from ~12 to 17 times chondrite abundance (Sun and McDonough, 1989). The incompatible and REE compositions of Group 3 metabasalts are well comparable with those of plume-type MORB (P-MORB) from many ophiolitic units of the Makran (Figs. 6c, d), as well as from many other localities. Accordingly, in the discrimination diagram in Figure 8, the Group 3 metabasalts plot close to the compositions for P-MORBs from various ophiolitic units of the North Makran (Saccani, 2015).

6. Discussion

6.1. Petrogenesis of the basaltic protoliths

The aim of this discussion is to identify the possible mantle sources and melting conditions for the magmatic protoliths of the Deyader blueschists in order to provide robust

constraints for the interpretation of their tectono-magmatic setting of formation. The three groups of volcanic protoliths described in Section 5 exhibit different trace elements contents (e.g., Zr, Y, Nb, Th) and REE patterns (Fig. 5), as well as different incompatible elements (e.g., Zr/Y, Y/Nb, Nb/Yb) and REE ratios (i.e., La_N/Yb_N, Sm_N/Yb_N, Sm_N/Dy_N) (Table 1, Fig. 7) suggesting that these rocks were originated from partial melting of chemically distinct mantle sources and/or different melting conditions. For example, relatively higher $(La/Yb)_N$ ratios may be due to high degree of partial melting of mantle sources enriched in La, or to low degree of partial melting in the spinel-facies of mantle sources comparatively less enriched in La, or again to partial melting in the garnet-facies of relatively depleted mantle sources (see Allègre and Minster, 1978; Pearce, 2008). Similar HREE contents (e.g., Yb_N = 14.2 -18.6, with values overlapping in the three group types; Table 1) but different LREE/HREE ratios (Table 1, Fig. 7a) suggest that the differences in the chemistry of their possible mantle sources most likely consisted in different enrichments in LREE, Zr, Nb, Th, and other incompatible elements. The Zr-Nb co-variation diagram in Figure 9a shows that Group1 and Group 2 volcanic protoliths of the Deyader blueschists were generated by partial melting of a depleted mantle source, whereas Group 3 rocks fit with a generation from an enriched or transitional mantle source (Le Roex et al., 1983). The diagram in Figure 9b further supports this conclusion. In fact, all the studied rocks plot along the mixing curve between N-MORB and OIB compositions with Group 1 and Group 2 metabasalts clustering between depleted (N-MORB) and slightly enriched (E-MORB) end member, and Group 3 metabasalts plotting towards the enriched OIB end member. In addition, a progressive increase of the enrichment from an OIB-type chemical component can be seen along the N-MORB-OIB mixing curve from Group 1 to Group 2 and Group 3 rocks (Fig. 9b). The Th-Nb co-variation (Fig.8) further points out for a genesis of the studied rocks from partial melting of mantle sources that have been influenced by enriched OIB-type chemical components prior to melting without any

contribution from subduction-related chemical components and/or continental crust contamination. The relatively high HREE contents (e.g., Yb_N = ~13 - ~17) in the rather primitive basaltic protoliths suggest no involvement of residual garnet in the mantle source. In fact, all samples plot in the MORB array in the TiO_2/Yb vs. Nb/Yb diagram (Fig. 10a), suggesting that they derived from partial melting in the spinel-facies mantle (Pearce, 2008).

Given these assumptions, we performed a semi-quantitative non-modal, batch partial melting models in order to make out the possible mantle peridotite compositions and melting conditions that can reproduce the compositions of the relatively most primitive basaltic protoliths for each geochemical group of blueschists. The non-modal, batch partial melting model was used because the melt generated can be considered as a "single batch" of magma, which is not depending on those factors controlling the segregation of the melts from the mantle. These factors (e.g., permeability threshold of the source) cannot be modeled in detail and therefore, this method better applies to semi-quantitative calculations (see Rollinson, 1993, p. 121). The magma chamber petrogenetic processes (e.g., fractional crystallization) cannot reliably be modeled because, due to the fragmented tectonic nature of the studied metaophiolites, co-magmatic relationships between different samples even of the same chemical group cannot be unequivocally proved. Nonetheless, the effects of fractional crystallization can be mitigated by considering in our model only the relatively most primitive basaltic protoliths and using elements whose contents are commonly assumed to largely depend on the composition of the mantle source and its degree of partial melting, rather than fractional crystallization (e.g., Allègre and Minster, 1978). Finally, the accurate definition of the various factors controlling partial melting (i.e., the composition of mantle sources, degrees and depths of partial melting, etc.) cannot quantitatively be made for tectonically dismembered metaophiolites. Therefore, we used different models based on incompatible

trace elements and REE in order to crosscheck the results obtained from each model (Figs. 10, 11).

We have previously shown that the composition of the volcanic protoliths of the Deyader blueschists strongly points out for a genesis from partial melting of sub-oceanic mantle sources that have experienced variable metasomatism from deep mantle OIB-type chemical components. Therefore, in our models we chose as a possible mantle source for the Group 1 rocks the depleted MORB mantle (DMM) of Workman and Hart (2005). The possible mantle sources for Group 2 and Group 3 metabasalts are assumed as a DMM metasomatized to various extents of enrichment by an OIB-type chemical component according to the models presented in Saccani et al., 2003; Bortolotti et al., 2018; Barbero et al., 2020b). In our models, we used the enriched mantle of Lustrino et al. (2002) as the metasomatizing chemical component. The modal compositions of the assumed mantle sources, their chemical composition, the melting proportions, and the REE and trace elements distribution coefficients used in the models are listed in Supplementary Table S2.

6.1.1. Group 1 rocks

The Nb/Yb vs. TiO_2/Yb model (Fig. 10b) shows that Group 1 metabasalts can be generated from the partial melting of sources with depleted composition as the DMM (Workman and Hart, 2005). The low TiO_2/Yb ratios characterizing the Group 1 metabasalts suggest partial melting in the spinel-facies mantle. Accordingly, the Nb/Yb vs. Th petrogenetic model suggests that the compositions of Group 1 relatively primitive metabasalts can be explained by partial melting of the DMM in the spinel-facies mantle. (Fig. 11a). The REE modeling resumed here as a plot of LREE/HREE (La/Yb) vs. MREE/HREE (Dy/Yb) ratios (Fig. 11b) well confirms these results clearly indicating that the REE composition of the

most primitive Group 1 metabasalts can be explained by 10-15% partial melting of the DMM source in the spinel-facies. The Zr vs. La model shows the same results as described above. Indeed, the Zr vs. La co-variation of the relatively primitive Group 1 metabasalts fits well with ~10-15% partial melting of the DMM source in the spinel facies.

6.1.2. Group 2 rocks

Group 2 basaltic protoliths show compositions that are slightly enriched in Th, Ta, Nb and LREE with respect to those of Group 1 equivalents (Table 1, Fig. 6). These rocks show very flat REE patterns resembling those of E-MORBs or OPBs (Fig. 6d). These features are compatible with either partial melting of a mantle source slightly more enriched than the DMM, or low degrees (less than 3-5%) of partial melting of a DMM source. However, if compared to Group 1 rocks, lower degrees of partial melting of the same DMM source will result in higher LREE/HREE (e.g., La/Yb) and LREE/MREE (e.g., La/Sm) ratios with similar MREE/HREE (e.g., Sm/Yb) ratios and Yb contents. Compared to Group 1 rocks, Group 2 metabasalts show higher La/Yb and La/Sm ratios, but also higher Sm/Yb ratios (Figs. 7a, b) at comparable Yb contents (Table 1). In addition, the Dy/Yb ratios and the Zr contents of these rocks cannot be explained by <5% partial melting degree of a DMM source (Figs. 11b, c). Therefore, we assume that Group 2 metabasalts were derived from partial melting of a mantle source slightly more enriched than the DMM rather than low degrees of partial melting of a DMM source. In fact, all the models used in this paper indicate that the composition of Group 2 metabasalts is compatible with 10-12% partial melting of a slightly enriched MORB mantle source (EMM) compared to the DMM source (Figs. 10b, 11a-c).

6.1.3. Group 3 rocks

Group 3 basaltic protoliths show compositions that are quite different from those of Group 1 and Group 2 metabasalts. They are enriched in Th, Ta, Nb, and LREE and show slightly lower HREE contents (Table 1, Fig. 6). Compared to Group 1 and Group 2 metabasalts, these rocks show much higher $(La/Yb)_N$, $(La/Sm)_N$, and $(Sm/Yb)_N$ ratios (Figs. 7a, b) and overall chemical features that cannot be explained with partial melting of either a DMM source or EMM source (see Fig. 10b as an example). The chemical features of Group 3 metabasalts clearly point out for a genesis from a mantle source (EM) fairly enriched in incompatible elements and LREE. Similar to other metabasaltic groups, the low TiO_2/Yb, and Nb/Yb ratios suggest partial melting in the spinel-facies mantle (Figs. 10a, 11a).

The Nb/Yb vs. TiO_2/Yb model (Fig. 10b) shows that Group 3 rocks can be generated by low degrees (2.5 - 5%) of partial melting of an enriched mantle source in the spinel-facies mantle. Accordingly, the same results are obtained using the Nb/Yb vs. Th petrogenetic model (Fig. 11a). Though with minor differences, the same results are obtained using both the REE model and the Zr vs. La model, which indicate that REE and Zr compositions of Group 3 metabasalts can be explained by 2.5 – 7% partial melting of the enriched mantle source in the spinel stability field (Figs. 11b, c).

6.2. Comparison with the North Makran ophiolitic and metaophiolitic units and tectono-magmatic significance

The geochemical data presented in this paper suggest that the volcanic protoliths of the Deyader blueschists are represented by MORB-type rocks, which range in composition from normal- to enriched- and plume-type MORB. Accordingly, the petrogenetic models suggest progressive enrichment of the sub-oceanic mantle sources by plume-type chemical

components (e.g., Th, Nb, LREE, Zr) from E-MORB to P-MORB protoliths. Similar compositional variations and plume-type variable influence have been observed in the other ophiolitic and metaophiolitic units of the North Makran (Ghazi et al., 2004; Hunziker, 2014; Moslempour et al., 2015; Saccani et al., 2018; Esmaeili et al., 2020; Barbero et al., 2020a, 2020b, 2021a, 2021b; Barbero, 2021; Pandolfi et al., 2021; Sepidbar et al., 2020). Therefore, regardless of the different metamorphic evolution recorded in the different units, a comparison between volcanic protoliths of the Deyader blueschists and mafic volcanic/metavolcanic rocks of other North Makran ophiolitic units can be very helpful for improving the knowledge on nature and composition of the Makran Neo-Tethys during Mesozoic times. Hereafter we briefly summarize the geochemical and petrogenetic context of the North Makran ophiolitic and metaophiolitic units, namely, the Band-e-Zeyarat, Fannuj-Maskutan, Durkan, and Bajgan units/complexes, as well as the Coloured Mélange.

6.2.1. A brief summary of geochemistry and petrogenesis of the North Makran ophiolites

The Band-e-Zeyarat sheeted dykes, and volcanic rocks are mainly represented by Late Jurassic - Early Cretaceous basalts showing either N-MORB or E-MORB affinities (Ghazi et al., 2004; Barbero et al., 2020b) (Figs. 12a, b). According to Barbero et al. (2020b), N-MORBs formed by partial melting of a depleted sub-oceanic mantle peridotite in the spinel-facies, whereas E-MORBs were formed by partial melting of a depleted sub-oceanic mantle peridotite that was metasomatized by OIB-type (plume-type) components. These conclusions are also confirmed by Nd, Pb, and Sr isotopic data, which indicate that the Band-e-Zeyarat ophiolite was derived from more or less enriched mid-ocean ridge basalt-like mantle sources (Ghazi et al., 2004). This ophiolite records, therefore, an Early Cretaceous plume-ridge interaction in the Makran Neo-Tethys (Ghazi et al., 2004; Barbero et al., 2020b).

The extrusive sequence of Fannuj-Maskutan ophiolites mainly consists of basaltic pillow lavas and lava flows. No consensus exists about the petrogenetic mechanisms and tectonic setting of formation of these ophiolites. Desmons and Beccaluva (1983) related the genesis of the mafic lavas from these ophiolites to a mid-ocean ridge setting. Based on close similarities with mid-ocean ridge basalts, such as relatively high Ti, P, Y contents, coupled with Nb depletion, Moslempour et al. (2015) suggested that they formed in a back-arc basin setting. In contrast, Sepidbar et al. (2020) suggested that these ophiolites show a petrogenetic evolution from early-stage IAT-like gabbros to later-stage E-MORB-like basalts (as evidenced in the Th-Ta-Hf diagram in Fig. 12a). Accordingly, the diagram in Fig. 12b (Pearce and Norry, 1979) shows that the Zr/Y – Zr co-variation of the Fannuj-Maskutan basalts is not compatible with a genesis from a depleted supra-subduction zone mantle. Rather, it is compatible with a genesis from a slightly enriched-type MORB mantle. The same conclusions can be seen in the TiO_2/Yb vs. Nb/Yb co-variation (Pearce, 2008; Fig. 10a), which shows that these basalts plot, together with all the E-MORBs, along the N-MORB-E-MORB array.

The Durkan Complex basalts and metabasalts have recently been interpreted as remnants of Late Cretaceous disrupted seamounts (Barbero et al., 2021a, 2021b). They display variable geochemistry ranging from transitional P-MORB to alkaline OIBs. These features are summarized in Fig. 12a where these rocks plot across the boundary between E-MORB and Alkaline basalts compositional fields. Likewise, the Zr/Y vs. Zr co-variation (Fig. 12b) shows that they plot in the within-plate oceanic field and are consistent with a genesis from enriched to very enriched mantle sources. In detail, petrogenetic models show that the Durkan basaltic rocks were generated from the partial melting of depleted sub-oceanic mantle source that was metasomatized by OIB-type (plume-type) chemical components in a within-plate oceanic setting (Barbero et al., 2021b). These authors suggested that the chemical differences between P-MORBs and OIBs can be interpreted by different combinations of OIB-type enrichment,

partial melting degree, and depths of melting. These conclusions imply that the oceanic lithosphere onto which the Durkan seamounts were forming was characterized by an important mantle plume activity in the Late Cretaceous (Barbero et al., 2021b).

The volcanic protoliths of the Late Jurassic to Early Cretaceous HP-LT metaophiolites of the Bajgan Complex consist of N-MORB, E-MORB, and OIB (Pandolfi et al., 2021) (Figs. 12a, b). Based on petrological and lithostratigraphic evidence, Pandolfi et al. (2021) suggested that the Bajgan Complex is represented by metaophiolites formed in different oceanic tectonic settings characterized by different compositions of their mantle sources (Pandolfi et al., 2021). N-MORB volcanic protoliths were generated in mid-ocean ridge settings from depleted mantle sources, the slightly enriched E-MORB volcanic protoliths were generated in plume-influenced mid-ocean ridge settings, and the enriched OIB-type protoliths were generated in within-plate seamounts associated with plume–type activity (Pandolfi et al., 2021).

The mafic volcanic rocks in the Coloured Mélange Complex consist of both subduction-related and subduction-unrelated rocks-types. Subduction-unrelated rocks-types include N-MORBs, E-MORBs, and Late Cretaceous P-MORBs, OPBs, and alkaline basalts, which have been interpreted as remnants of the Mesozoic Neo-Tethys sector located between the Arabian plate and the Lut block (Saccani et al., 2018; Esmaeili et al., 2020, 2021). The occurrence of OPBs strongly point out for a Late Cretaceous mantle plume activity in this Neo-Tethys sector (Saccani et al., 2018). Likewise, Esmaeili et al. (2020) suggested that E-MORBs, P-MORBs, and alkaline basalts were formed from partial melting of a highly heterogeneous mantle source, which was extensively metasomatized by deep mantle OIB-type components and were thus erupted in a mid-ocean ridge featuring plume-ridge interaction.

6.2.2. Tectono-magmatic significance of the Deyader blueschists

In summary, the different ophiolitic and metaophiolitic units of the North Makran Domain represent fragments of both an oceanic crust that was forming in chemically composite mid-ocean ridge segments and oceanic within-plate seamounts. This oceanic crust developed from the Late Jurassic/Early Cretaceous to the Late Cretaceous and was largely characterized by mantle plume activity. As a general tendency, we can observe a magmatic evolution from depleted N-MORB and slightly enriched E-MORB compositions (e.g., Band-e-Zeyarat ophiolites; Ghazi et al., 2004; Barbero et al., 2020b) to comparatively more enriched P-MORB and alkaline OIB compositions (e.g., Durkan Complex; Barbero et al., 2021a, 2021b) from the Late Jurassic – Early Cretaceous to Late Cretaceous, suggesting an increasing influence of the mantle plume activity toward Late Cretaceous times (see also Barbero et al., 2021b). Though strongly metamorphosed and undated, the Deyader blueschists fit very well with the general context of formation of the North Makran ophiolites and metaophiolites. In fact, they show the same compositional varieties (i.e., N- MORB, E-MORB, P-MORB) observed in the Bajgan Complex (Figs. 12a, b), as well as similar petrogenetic processes (see Pandolfi et al., 2021). It is worth to note that the Deyader Metamorphic Complex and the Bajgan Complex, different from other Makran ophiolitic and metaophiolitic units, also show similar metamorphic peak in the blueschists facies conditions (Hunziker et al., 2017; Pandolfi et al., 2021). In addition, the Deyader blueschists show compositions, petrogenetic processes, and tectono-magmatic setting of formation, which are very similar also to equivalent rocks forming the Band-e-Zeyarat, Fannuj-Maskutan, and Durkan ophiolites, as well as most of the ophiolitic rocks included in the Coloured Mélange. In detail, N-MORB rocks similar to Group 1 blueschist protoliths are found in the Band-e-Zeyarat Unit and in the Coloured Mélange. E-MORBs like those of Group 2 blueschist

protoliths are found in the Band-e-Zeyarat and Fannuj-Maskutan Units, as well as in the Coloured Mélange; P-MORBs similar to Group 3 blueschist protoliths are found in the Durkan Unit and the Coloured Mélange (Figs. 12a, b). This allows us to conclude that the magmatic protoliths of the Deyader blueschists, similar to all the other ophiolitic and metaophiolitic units of the North Makran Domain, represent fragments of a unique Late Jurassic – Cretaceous oceanic basin that was strongly affected by mantle plume activity and plume-ridge interaction. It interesting to note that mantle plume activity most likely affected the Middle East Neo-Tethys at a regional scale since Late Jurassic times, as recorded in the northern sector of Sanandaj-Sirjan Zone (Azizi et al., 2018a, b). A possible tectono-magmatic scenario in which the Deyader magmatic protoliths, along with similar volcanic rocks from the ophiolitic and metaophiolitic units of the North Makran Domain, were generated and erupted is shown in Fig. 13a, whereas a schematic paleogeographic map of the Middle East sector of the Neo-Tethys in Late Cretaceous times is shown in Fig. 13b. This model implies the early formation of N-MORBs in a mid-ocean ridge without any influence of plume-type components. The progressive uprising of mantle plume material from Early to Late Cretaceous (Barbero et al., 2021b) resulted in increasing plume-ridge interaction with formation of E-MORBs and P-MORBs in plume-proximal mid-ocean ridges. The mantle plume activity peaked in the formation of alkaline basalts in seamount settings during the Late Cretaceous (Fig. 13b).

7. Conclusions

The Deyader Metamorphic Complex represents a tectonic element of the North Makran Domain and consists of tectonic slices of low-grade metasedimentary rocks and HP-LT

blueschists derived from mafic protoliths. Blueschists tectonic slices are subordinate in volume and are tectonically juxtaposed onto the low-grade metasedimentary rocks. The geochemical and petrogenetic study on blueschists derived from volcanic protoliths, as well as a geochemical comparison with other North Makran ophiolites allows the following conclusion to be drawn:

1) The volcanic protoliths are represented by basaltic rocks. Based on whole rock geochemical features, basaltic rocks consist of sub-alkaline basalts showing both N-MORB (Group 1) and E-MORB (Group 2) compositions, as well as transitional basalts showing P-MORB composition (Group 3).

2) Petrogenetic models based on several incompatible elements, such as REE, Th, Nb, Zr, Y, and Ti indicate that the Deyader basaltic protoliths derived from partial melting in the spinel-facies of a sub-oceanic mantle metasomatized to various extents by an OIB-type (plume-type) chemical component. In detail, N-MORB, E-MORB, and P-MORB derived from a pure DMM source, from a DMM source slightly enriched by plume-type components, and from a DMM source significantly enriched by plume-type components, respectively.

3) Basaltic protoliths of the Deyader blueschists show the same compositions and petrogenetic mechanisms observed in basaltic rocks from other ophiolitic and metaophiolitic units from the North Makran Domain.

4) Though the age of the basaltic protoliths of the Deyader blueschists cannot be determined, this very close geochemical similarity and regional evidence allow us to suggest that the Deyader blueschists along with all the ophiolitic and metaophiolitic units of the North Makran Domain, represent fragments of a unique Late Jurassic – Cretaceous oceanic basin that was strongly affected by mantle plume activity and different extents of plume-ridge interaction.

Acknowledgment

The research has been funded by: Darius Project (Head M. Marroni), PRA project of the Pisa University (Head S. Rocchi), IGG-CNR, FAR-2018 Project of the Ferrara University (Head E.S.). Mr. Ahmad Behboodi is sincerely thanked for his appreciated assistance in organizing field work. Constructive and thorough reviews for the Journal by F. Lucci and an anonymous reviewer, as well as valuable suggestions by the Editor I. Uysal have helped us improve the science and organization presented in the paper.

References

Allahyari, K., Saccani, E., Rahimzadeh, B., Zeda, O., 2014. Mineral chemistry and petrology of highly magnesian ultramafic cumulates from the Sarve-Abad (Sawlava) ophiolites (Kurdistan, NW Iran): New evidence for boninitic magmatism in intra-oceanic fore-arc setting in the Neo-Tethys between Arabia and Iran. Journal of Asian Earth Sciences 79, 312–328, doi: 10.1016/j.jseaes.2013.10.005.

Allègre, C.J., Minster, J.F., 1978. Quantitative models of trace element behavior in magmatic processes. Earth Planet. Sci. Lett. 38, 1-25.

Azizi, H., Nouri, F., Stern, R.J., Azizi, M., Lucci, F., Asahara, Y., Zarinkoub, M.H., Chung S.L., 2020. New evidence for Jurassic continental rifting in the northern Sanandaj Sirjan

Zone, western Iran: the Ghalaylan seamount, southwest Ghorveh. International Geology Review, 62, 1635-1657, doi: 10.1080/00206814.2018.1535913.

Azizi, H., Lucci, F., Stern, R.J., Hasannejad, S., Asahara, Y., 2018. The Late Jurassic Panjeh submarine volcano in the northern Sanandaj-Sirjan Zone, northwest Iran: Mantle plume or active margin? Lithos, 308–309, 364-380, doi: 10.1016/j.lithos.2018.03.019.

Barbero, E., 2021. Geological and petrological investigation of the western North Makran ophiolites (SE Iran): new constraints for the Late Jurassic-Cretaceous tectono-magmatic and geodynamic evolution of the Neo-Tethys Ocean. University of Ferrara, Italy, p. 324.

Barbero, E., Delavari, M., Dolati, A., Saccani, E., Marroni, M., Catanzariti, R., Pandolfi, L., 2020a. The Ganj Complex reinterpreted as a Late Cretaceous volcanic arc: Implications for the geodynamic evolution of the North Makran domain (southeast Iran). Journal of Asian Earth Science, https://doi.org/10.1016/j.jseaes.2020.104306.

Barbero, E., Delavari, M., Dolati, A., Vahedi, L., Langone, A., Marroni, M., Pandolfi, L., Zaccarini, F., Saccani, E., 2020b. Early Cretaceous Plume–Ridge Interaction Recorded in the Band-e-Zeyarat Ophiolite (North Makran, Iran): New Constraints from Petrological, Mineral Chemistry, and Geochronological Data. Minerals 10, 1100, doi:10.3390/min10121100.

Barbero, E., Pandolfi, L., Delavari, M., Dolati, A., Saccani, E., Catanzariti, R., Lucani, V., Chiari, M., Marroni, M., 2021a. The western Durkan Complex (Makran Accretionary Prism, SE Iran): A Late Cretaceous tectonically disrupted seamounts chain and its role in controlling deformation style. Geoscience Frontiers 12, 101106, https://doi.org/10.1016/j.gsf.2020.12.001.

Barbero E., Zaccarini, F., Delavari M., Dolati A., Saccani E., Marroni M. and Pandolfi L. 2021b. New evidence for Late Cretaceous plume-related seamounts in the Middle East sector of the Neo-Tethys: Constraints from geochemistry, petrology, and mineral

chemistry of the magmatic rocks from the western Durkan Complex (Makran Accretionary Prism, SE Iran). Lithos 396–397, https://doi.org/10.1016/j.lithos.2021.106228.

Barrier, E., Vrielynck, B., Brouillet, J.F., Brunet, M.F., 2018. Paleotectonic Reconstruction of the Central Tethyan Realm. Tectono-Sedimentary-Palinspastic maps from Late Permian to Pliocene. Atlas of 20 maps (scale: 1:15.000.000). CCGM/CGMW, Paris, http://www.ccgm.org.

Bortolotti, V., Chiari, M., Goncuoglu, M.C., Principi, G., Saccani, E., Tekin, U.K., Tassinari, R., 2018. The Jurassic–Early Cretaceous basalt–chert association in the ophiolites of the Ankara Mélange, east of Ankara, Turkey: age and geochemistry. Geological Magazine 155: 451-478, doi: https://doi.org/10.1017/S0016756817000401.

Burg, J.-P., 2018. Geology of the onshore Makran accretionary wedge: Synthesis and tectonic interpretation. Earth Science Reviews 185, 1210-1231, https://doi.org/10.1016/j.earscirev.2018.09.011.

Burg, J.-P., Bernoulli, D., Smit, J., Dolati, A., Bahroudi, A., 2008. A giant catastrophic mud-and-debris flow in the Miocene Makran. Terra Nova 20, 188-193.

Burg, J.-P., Dolati, A., Bernoulli, D., Smit, J., 2013. Structural style of the Makran tertiary accretionary complex in SE Iran. In: Al Hosani, K., Roure, F., Ellison, R., Lokier, S. (Eds.), Lithosphere Dynamics and Sedimentary Basins: The Arabian Plate and Analogues. Frontiers in Earth Sciences vol.5. Springer, Berlin, Heidelberg, pp. 239-259.

Delavari, M., Dolati, A., Marroni, M., Pandolfi, L., Saccani E., 2016. Association of MORB and SSZ ophiolites along the shear zone between Coloured Mélange and Bajgan Complexes (North Maran, Iran): Evidence from the Sorkhband area. Ofioliti 41, 21-34.

Delaloye, M., Desmons, J., 1980. Ophiolites and mélange terranes in Iran: A geochronological study and its paleotectonic implications. Tectonophysics 68, 83-111.

Dercourt, J., Zonenshian, L.P., Ricou, L.E., Kazmin, V.G., LePichon, X., Knipper, A.L., Grandjacquet, C., Sbortshikov, M., Geyssant, J., Lepvrier, C., Pechersky, D.H., Boulin, J., Sibuet, J.C., Savostin, L.A., Sorokhtin, O., Westphal, M., Bazhenov, M.L., Lauer, J.P., Biju-Duval, B., 1986. Geological evolution of the Tethys Belt from the Atlantic to the Pamir since the Lias. Tectonophysics 123, 241-315.

Desmons, J., Beccaluva, L., 1983. Mid-Ocean ridge and island-arc affinities in ophiolites from Iran: Palaeographic implications. Chemical Geology 39, 39-63.

Dilek, Y., Furnes, H., 2011. Ophiolite genesis and global tectonics: geochemical and tectonic fingerprinting of ancient oceanic lithosphere. Geological Society of America Bulletin 123, 387-411.

Dolati, A., 2010. Stratigraphy, Structure Geology and Low-temperature Thermochronology Across the Makran Accretionary Wedge in Iran. (PhD Thesis). ETH Zurich, pp. 165.

Dolati, A., Burg, J.-P., 2013. Preliminary fault analysis and paleostress evolution in the Makran Fold-and-Thrust Belt in Iran. In: Al Hosani, K., Roure, F., Ellison, R., Lokier, S. (Eds.), Lithosphere Dynamics and Sedimentary Basins: The Arabian Plate and Analogues. Frontiers in Earth Sciences, Springer, Heidelberg, pp. 261–277. https://doi.org/10.1007/978-3-642-30609-9_13

Dorani, M., Arvin, M., Oberhänsli, R., Dargahi, S., 2017. P-T evolution of metapelites from the Bajgan complex in the Makran accretionary prism, south eastern Iran. Geochemistry 77, 459–475. https://doi.org/10.1016/j.chemer.2017.07.004.

Eftekhar-Nezhad, J., Arshadi, S., Mahdavi, M.A., Morgan, K.H., McCall, G.J.H., Huber, H., 1979. Fannuj Quadrangle Map 1:250000. Ministry of Mines and Metal, Geological Survey of Iran, Tehran.

Esmaeili, R., Xiao, W., Ebrahimi, M., Zhang, J.E., Zhang, Z., El-Rahman, Y.A., Han, C., Wan, B., Ao, S., Song, D., Shahabi, S., Aouizerat, A., 2020. Makran ophiolitic basalts

(SE Iran) record Late Cretaceous Neotethys plume-ridge interaction. International Geology Review 62, 1677-1697, doi: 10.1080/00206814.2019.1658232.

Esmaeili, R., Ao, S., Shafaii Moghadam, H., Zhang, Z., Griffin, W.L., Ebrahimi, M., Xiao, W., Wan, B., Bhandari, S., 2021. Amphibolites from Makran accretionary complex record Permian-Triassic Neo-Tethyan evolution. International Geology Review, https://doi.org/10.1080/00206814.2021.1946663

Ghazi, A.M., Hassanipak, A.A., Mahoney, J.J., Duncon R.A., 2004. Geochemical characteristics, 40Ar-39Ar ages and original tectonic setting of the Band-e-Zeyarat/Dar Anar ophiolite, Makran accretionary Prism, S.E. Iran. Tectonophysics 193, 175-196.

Hunziker, D., 2014. Magmatic and metamorphic history of the North Makran ophiolites and blueschists (SE Iran): Influence of Fe3+/Fe2+ ratios in blueschist facies minerals on geothermobarometric calculations. Doctoral dissertation. Eidgenössische Technische Hochschule ETH Zürich, no. 21778.

Hunziker, D., Burg, J.-P., Bouilhol, P., von Quadt, A., 2015. Jurassic rifting at the Eurasian Tethys margin: Geochemical and geochronological constraints from granitoids of North Makran, southeastern Iran. Tectonics 34, 571-593.

Hunziker, D., Burg, J.-P., Moulas, E., Reusser, E., Omrani, J., 2017. Formation and preservation of fresh lawsonite: Geothermobarometry of the North Makran Blueschists, southeast Iran. Journal of Metamorphic Geology 35, 871–895, doi: 10.1111/jmg.12259.

Khan, S.R., Jan, M.Q., Khan, T., Khan, A.M., 2007. Petrology of the dykes from the Waziristan Ophiolite, NW Pakistan, Journal of Asian Earth Sciences 29, 369-377, doi: 10.1016/j.jseaes.2006.08.001

Kopp, C., Fruehn, J., Flueh, E.R., Reichert, C., Kukowski, N., Bialas, J., Klaeschen, D., 2000. Structure of the Makran subduction zone from wide-angle and reflection seismic data. Tectonophysics 329, 171–191, https://doi.org/10.1016/S0040-1951(00)00195-5

Lachance, G.R., Trail, R.J., 1966. Practical solution to the matrix problem in X-ray analysis. Canadian Spectroscopy 11, 43-48.

Le Roex, A.P., Dick, H.J.B., Erlank, A.J., Reid, A.M., Frey, F.A., Hart, S.R., 1983. Geochemistry, Mineralogy and Petrogenesis of Lavas Erupted along the Southwest Indian Ridge Between the Bouvet Triple Junction and 11 degrees East. Journal of Petrology 24, 267-318.

Lustrino, M., Melluso, L., Morra, V., 2002. The transition from alkaline to tholeiitic magmas: a case study from the Orosei-Dorgali Pliocene volcanic district (NE Sardinia, Italy). Lithos 63, 83–113.

McCall, G.J.H., 2002. A summary of the geology of the Iranian Makran. The Tectonic and Climatic Evolution of the Arabian Sea Region. In: Clift, P.D., Kroon, D., Gaedicke, C., Craig, J. (Eds.), Geological Society of London Special Publications 195, 147-204.

McCall, G.J.H., Kidd, R.G,W., 1982. The Makran southeastern Iran: the anatomy of a convergent margin active from Cretaceous to present. In: Leggett, J.K. (Ed.), Trench-forearc geology: sedimentation and tectonics of modern and ancient plate margins. Vol 10, 387-397.

Moghadam, H.S., Arai, S., Griffin, W.L., Khedr, M., Saccani, E., Henry, H., O'Reilly, S.Y., Ghorbani, G., 2022. Geochemical variability among stratiform chromitites and ultramafic rocks from Western Makran, South Iran. Lithos, https://doi.org/10.1016/j.lithos.2021.106591.

Mohammadi, A., Burg, J.-P., Winkler, W., Ruh, J., von Quadt, A., 2016. Detrital zircon and provenance analysis of Late Cretaceous–Miocene onshore Iranian Makran strata: Implications for the tectonic setting. Geological Society of America Bulletin 128, 1481–1499. https://doi.org/10.1130/B31361.1

Monsef, I., Rahgoshay, M., Pirouz, M., Chiaradia, M., Grégoire, M., Ceuleneer, G., 2019. The Eastern Makran Ophiolite (SE Iran): evidence for a Late Cretaceous fore-arc oceanic crust. International Geology Review 61, 1313–1339. https://doi.org/10.1080/00206814.2018.1507764.

Moslempour, M.E., Khalatbari-Jafari, M., Ghaderi, M., 2015. Petrology, Geochemistry and Tectonics of the Extrusive Sequence of Fannuj-Maskutan Ophiolite, Southeastern Iran. Journal Geological Society of India 85, 604-618.

Pandolfi, L., Barbero, E., Marroni, M., Delavari, M., Dolati, A., Di Rosa, M., Frassi, C., Langone, A., Farina, F., MacDonald, C.S., Saccani, E., 2021. The Bajgan Complex revealed as a Cretaceous ophiolite-bearing subduction complex: A key to unravel the geodynamics of Makran (southeast Iran). Journal of Asian Earth Sciences, 222, https://doi.org/10.1016/j.jseaes.2021.104965

Pearce J.A., 1996. A user's guide to basalt discrimination diagrams. In: Bailes, A.H., Christiansen, E.H., Galley, A.G., Jenner, G.A., Keith, J.D., Kerrich, R., Lentz, D.R., Lesher, C.M., Lucas, S.B., Ludden, J.N., Pearce, J.A., Peloquin, S.A., Stern, R.A., Stone, W.E., Syme, E.C., Swinden, H.S., Wyman, D.A. (Eds.), Trace element geochemistry of volcanic rocks: applications for massive sulphide exploration. Short Course Notes. Geological Association of Canada 12, 79-113.

Pearce, J.A., 2008. Geochemical fingerprinting of oceanic basalts with applications to ophiolite classification and the search for Archean oceanic crust. Lithos 100, 14–48, https://doi.org/10.1016/j.lithos.2007.06.016.

Pearce, J.A., Norry, M.J., 1979. Petrogenetic implications of Ti, Zr, Y, and Nb variations in volcanic rocks. Contributions to Mineralogy and Petrology 69, 33-47.

Pirnia, T., Saccani, E., Torabi, G., Chiari, M., Gorican, S., Barbero, E., 2020. Cretaceous tectonic evolution of the Neo-Tethys in Central Iran: Evidence from petrology and age

of the Nain-Ashin ophiolitic basalts. Geoscience Frontiers 11, 57–81, https://doi.org/10.1016/j.gsf.2019.02.008

Rollnson, H., 1993. Using geochemical data: evaluation, presentation, interpretation. Longman, London, 352 p.

Saccani, E., 2015. A new method of discriminating different types of post-Archean ophiolitic basalts and their tectonic significance using Th-Nb and Ce-Dy-Yb systematics. Geoscience Frontiers 6, 481-501.

Saccani, E., Photiades, A., Padoa, E., 2003. Geochemistry, petrogenesis and tectono-magmatic significance of volcanic and subvolcanic rocks from the Koziakas Mélange (Western Thessaly, Greece). Ofioliti 28, 43-57.

Saccani, E., Delavari, M., Dolati, A., Marroni, M., Pandolfi, L., Chiari, M., Barbero E., 2018. New insights into the geodynamics of Neo-Tethys in the Makran area: Evidence from age and petrology of ophiolites from the Coloured Mélange Complex (SE Iran). Gondwana Research 62, 306-327.

Şengör, A.M.C., 1990. A new model for the Late Paleozoic-Mesozoic tectonic evolution of Iran and implications for Oman. The Geology and Tectonics of the Oman Region. In: Robertson, A.H.F., Searle, M.P., Ries, A.C. (Eds), Geological Society London Special Publication 49, 797-831.

Sepidbar, F., Lucci, F., Biabangard, H., Zaki Khedr, M., Jiantang, P., 2020. Geochemistry and tectonic significance of the Fannuj-Maskutan SSZ-type ophiolite (Inner Makran, SE Iran). International Geology Review 62, 2077-2104, https://doi.org/10.1080/00206814.2020.1753118.

Stampfli, G., Marcoux, J., Baud, A., 1991. Tethyan margins in space and times. Palaeogeography Palaeoclimatology Palaeoecology 87, 373-409.

Sun, S.S., McDonough, W.F., 1989. Chemical and isotopic systematics of oceanic basalts: implications for mantle composition and processes. In: Saunders, A.D., Norry, M.J. (Eds.), Magmatism in the Ocean Basins. Geological Society of London Special Publication 42, 313-345.

Winchester, J.A., Floyd, P.A., 1977. Geochemical discrimination of different magma series and their differentiation products using immobile elements. Chemical Geology 20, 325-343.

Wood, D.A., 1980. The application of a Th-Hf-Ta diagram to problems of tectonomagmatic classification and to establishing the nature of crustal contamination of basaltic lavas of the British Tertiary volcanic province. Earth and Planetary Science Letters 50, 11-30.

Workman, R.K., Hart, S.R., 2005. Major and trace element composition of the depleted MORB mantle (DMM). Earth and Planetary Science Letters 231, 53-72.

Table captions

Table 1. Major (wt.%) and trace (ppm) element composition of metavolcanic blueschists from the Deyader Metamorphic Complex. Abbreviations: XRF: X-ray fluorescence spectrometry; ICP-MS: inductively coupled plasma-mass spectrometry; n.d.: not detected. Mg# = 100 x MgO / (MgO + FeO). Fe_2O_3 = 0.15 x FeO. Normalizing values for REE ratios from Sun and McDonough (1989). See Figure 2 for sample location.

Figure caption

Figure 1. a) Simplified tectonic sketch map of the Iranian-Afghan-Pakistani area (modified from Khan et al., 2007; Allahyari et al., 2014; Mohammadi et al., 2016; Pirnia et al., 2020); b) simplified geological map of the North Makran Domain showing the different tectono-stratigraphic units (modified from Eftekhar-Nezhad et al., 1979; Burg, 2018; Barbero et al., 2021b, and references therein).

Figure 2. Simplified geological map of the Deyader Metamorphic Complex and surrounding tectonic units (modified from Hunziker et al., 2017). Sampling locations are identified in Figure with short labels. The correspondence between samples and short labels is given in Table 1.

Figure 3. Field photographs of the different blueschist types in the Deyader Metamorphic Complex. a) metapillow lavas with well-preserved pillow structures and intra-pillow marble; b) metapillow lavas with well-preserved pillow structures and large bodies of marble; c), d) fine-grained massive blueschists (c: large view, d: close view); e) coarse-grained massive blueschists characterized by cm-thick compositional layering (highlighted by dashes lines). The inset e_1) shows the coarse-grained texture of these rocks; f) metavolcano-sedimentary sequences characterized by the alternation of thin (few cm) layers of metalavas and meta-volcaniclastic arenites, as well as by the occurrence of layers of metapillow lavas. The whiteboard in panels a), c), and f) shows both inch (vertical) and centimetre (horizontal) scales. The circle in panel b) indicate the hammer used for scale.

Figure 4. Microphotos showing the main textures and mineral phase of the blueschists from the Deyader Metamorphic Complex. Abbreviations. PPL: plane polarized light; XPL: crossed polarized light; Aln: allanite; Amp: amphibole (generic); Chl: chlorite; Gln: glaucophane; Lws: lawsonite; Pnp: pumpellyite; Qz: quartz; Ttn: titanite; repl: replacement along rims and cracks. The white box in panel e) indicates the area shown in panel f).

Figure 5. Nb/Y vs. Zr/Ti discrimination diagram of Winchester and Floyd (1977) modified by Pearce (1996) for metavolcanic blueschists from the Deyader Metamorphic Complex. The compositions of different rock types from various ophiolitic units of the North Makran domain are shown for comparison (data from Ghazi et al., 2004; Saccani et al., 2018; Sepidbar et al., 2020; Barbero et al., 2020b, 2021b; Pandolfi et al., 2021). Abbreviations, N-MORB: normal-type mid-ocean ridge basalt; OPB: oceanic plateau basalt; E-MORB: enriched-type mid-ocean ridge basalt; P-MORB: plume-type mid-ocean ridge basalt; OIB: alkaline oceanic within-plate basalt.

Figure 6. N-MORB normalized incompatible element patterns and Chondrite-normalized rare earth element patterns for metavolcanic blueschists from the Deyader Metamorphic Complex. Normalizing values are from Sun and McDonough (1989). Compositions of typical N-MORB, E-MORB, and alkaline oceanic within-plate basalt (OIB) are from Sun and McDonough (1989), respectively. The compositions of different rock types from various ophiolitic units of the North Makran domain are shown for comparison (data from Ghazi et al., 2004; Saccani et al., 2018; Sepidbar et al., 2020; Barbero et al., 2020b, 2021b; Pandolfi et al., 2021). Abbreviations, N-MORB: normal-type mid-ocean ridge basalt; OPB: oceanic

plateau basalt; E-MORB: enriched-type mid-ocean ridge basalt; P-MORB: plume-type mid-ocean ridge basalt; OIB: alkaline oceanic within-plate basalt.

Figure 7. Chondrite-normalized $(La/Sm)_N$ vs. $(La/Yb)_N$ (a) and $(Sm/Yb)_N$ vs. $(Sm/Yb)_N$ (b) diagrams for metavolcanic blueschists from the Deyader Metamorphic Complex. Normalizing values are from Sun and McDonough (1989). The compositions of different rock types from various ophiolitic units of the North Makran domain are shown for comparison (data from Ghazi et al., 2004; Saccani et al., 2018; Sepidbar et al., 2020; Barbero et al., 2020b, 2021b; Pandolfi et al., 2021). Abbreviations, N-MORB: normal-type mid-ocean ridge basalt; OPB: oceanic plateau basalt; E-MORB: enriched-type mid-ocean ridge basalt; P-MORB: plume-type mid-ocean ridge basalt; OIB: alkaline oceanic within-plate basalt.

Figure 8. N-MORB normalized Th vs. Nb discrimination diagram of Saccani (2015) for metavolcanic blueschists from the Deyader Metamorphic Complex. Vectors indicate the trends of compositional variations due to the main petrogenetic processes. The compositions of different rock types from various ophiolitic units of the North Makran domain are shown for comparison (data from Ghazi et al., 2004; Saccani et al., 2018; Sepidbar et al., 2020; Barbero et al., 2020b, 2021b; Pandolfi et al., 2021). Abbreviations, N-MORB: normal-type mid-ocean ridge basalt; OPB: oceanic plateau basalt; E-MORB: enriched-type mid-ocean ridge basalt; P-MORB: plume-type mid-ocean ridge basalt; OIB: alkaline oceanic within-plate basalt; AFC: assimilation-fractional crystallization; OIB-CE: ocean island-type (plume-type) component enrichment; FC: fractional crystallization. Normalizing values, as well as the composition of typical N-MORB, E-MORB, and OIB (stars) are from Sun and McDonough (1989).

Figure 9. a) Nb vs. Zr (modified from Barbero et al., 2021b) and b) Zr/Y vs. Zr/Nb diagrams for metavolcanic blueschists from the Deyader Metamorphic Complex. The dashed line in b) represents the mixing curve calculated using OIB and N-MORB endmembers (from Le Roex et al. 1983). The compositions of different rock types from various ophiolitic units of the North Makran domain are shown for comparison (data from Ghazi et al., 2004; Saccani et al., 2018; Sepidbar et al., 2020; Barbero et al., 2020b, 2021b; Pandolfi et al., 2021). Abbreviations, N-MORB: normal-type mid-ocean ridge basalt; OPB: oceanic plateau basalt; E-MORB: enriched-type mid-ocean ridge basalt; P-MORB: plume-type mid-ocean ridge basalt; OIB: alkaline oceanic within-plate basalt.

Figure 10. a) TiO_2/Yb vs. Nb/Yb diagram (Pearce, 2008) for metavolcanic blueschists from the Deyader Metamorphic Complex. The compositions of different rock types from various ophiolitic units of the North Makran domain are shown for comparison (data from Ghazi et al., 2004; Saccani et al., 2018; Sepidbar et al., 2020; Barbero et al., 2020b, 2021b; Pandolfi et al., 2021). Abbreviations, N-MORB: normal-type mid-ocean ridge basalt; OPB: oceanic plateau basalt; E-MORB: enriched-type mid-ocean ridge basalt; P-MORB: plume-type mid-ocean ridge basalt; OIB: alkaline oceanic within-plate basalt. b) Inset showing the isobaric (2.5 Gpa) melting curves for different mantle sources: DMM (depleted MORB mantle), EMM (enriched MORB mantle, and EM (enriched mantle). DMM composition is from Workman and Hart (2005), EMM and EM represent theoretical mantle sources calculated by assuming different degrees of enrichment by an OIB-type chemical component (Lustrino et al., 2002) of the DMM. Only the relatively less fractionated metabasalts of each rock type are shown.

Figure 11. Nb/Yb vs. Th (a), Dy/Yb vs. La/Yb (b), and Zr vs. La (c) batch melting

curves for different mantle sources: DMM (depleted MORB mantle), slightly enriched MORB mantle, and enriched mantle. DMM composition is from Workman and Hart (2005), EMM and EM represent theoretical mantle sources calculated by assuming different degrees of enrichment by an OIB-type chemical component (from Lustrino et al., 2002) of the DMM. Melting curves are calculated for spinel-facies conditions following Saccani et al. (2003); Bortolotti et al. (2018); Barbero et al. (2020b). Input parameters (source modes, melting proportions, and partition coefficients, source compositions) for batch melting models are given in Supplementary Table S2. Only the relatively less fractionated metabasalts of each rock type are shown.

Figure 12. Comparison between the composition of metavolcanic blueschists from the Deyader Metamorphic Complex and mafic volcanic and metavolcanic rocks from several ophiolitic units of the North Makran (data from Ghazi et al., 2004; Saccani et al., 2018; Sepidbar et al., 2020; Barbero et al., 2020b, 2021b; Pandolfi et al., 2021). a) Th-Ta-Hf/3 (Wood, 1980) discrimination diagram; b) Zr/Y vs. Zr diagram (Pearce and Norry, 1979). Abbreviations, N-MORB: normal-type mid-ocean ridge basalt; E-MORB: enriched-type mid-ocean ridge basalt; WPB: within-plate basalt; PM: primordial mantle (Sun and McDonough, 1989); DMM: depleted MORB mantle (Workman and Hart, 2005); SSZM: depleted supra-subduction zone mantle. Partial melting paths from PM, DMM, and SSZM are calculated based on Pearce and Norry (1979), Saccani et al. (2003), and Bortolotti et al. (2018).

Figure 13. a) Cartoon showing the tectono-magmatic model for the petrogenesis of the magmatic protoliths of the Deyader blueschists within the Makran sector of the Neo-Tethys, which could also apply to the entire North Makran ophiolitic and metaophiolitic units. Uprising of melts from the mantle, as well as styles of both intrusions and eruptions are not

shown in detail. b) Paleogeographic map of the Neo-Tethys Ocean and surrounding continental domains in the Middle East area in the Late Cretaceous (modified from Mohammadi et al., 1990; Barrier et al., 2018 and based on data from Esmaeili et al., 2020, 2021; Pirnia et al., 2020; Barbero et al., 2021a, 2021b; Moghadam et al., 2022; Pandolfi et al., 2021). Abbreviations in Panel 13b, CIM: Central Iran Microcontinent; NS: Nain - Sabzevar Ocean; SBB: Share Babak - Baft Ocean.

Figure 1 color for Online only

Click here to access/download;Figure;Fig_01.jpg

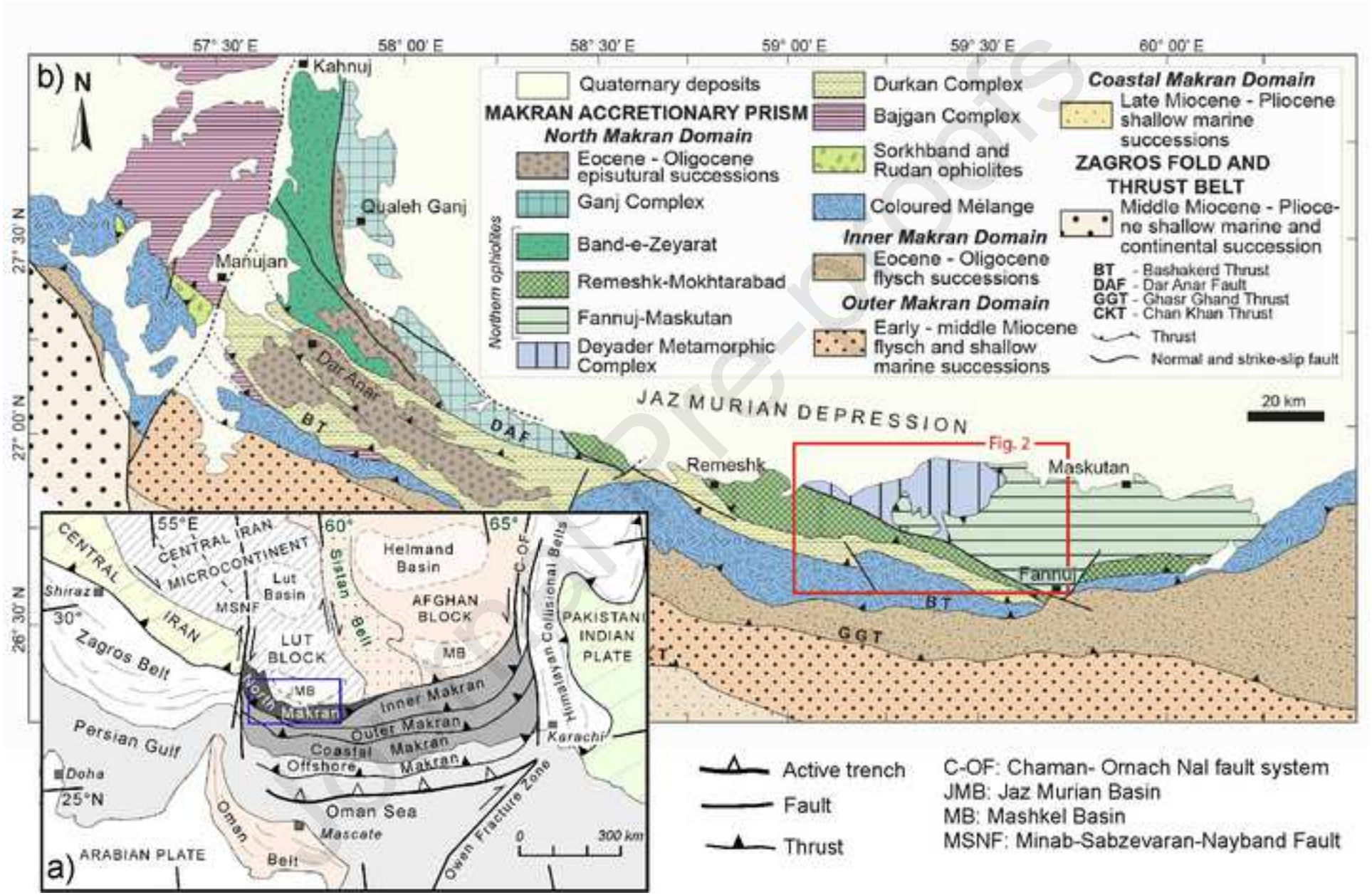

Figure 2 color revised for Online only

Click here to access/download;Figure;Fig_02_R.jpg

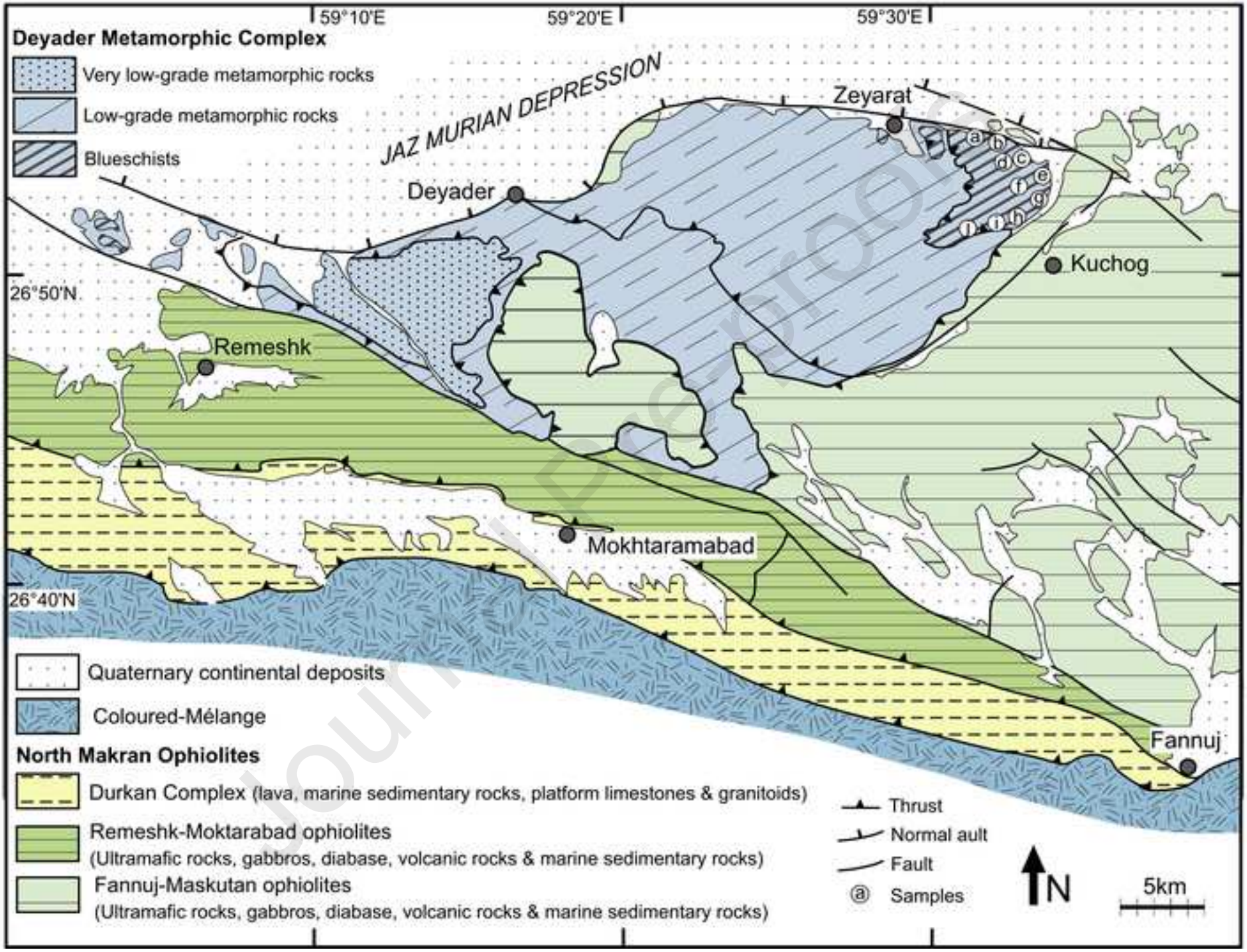

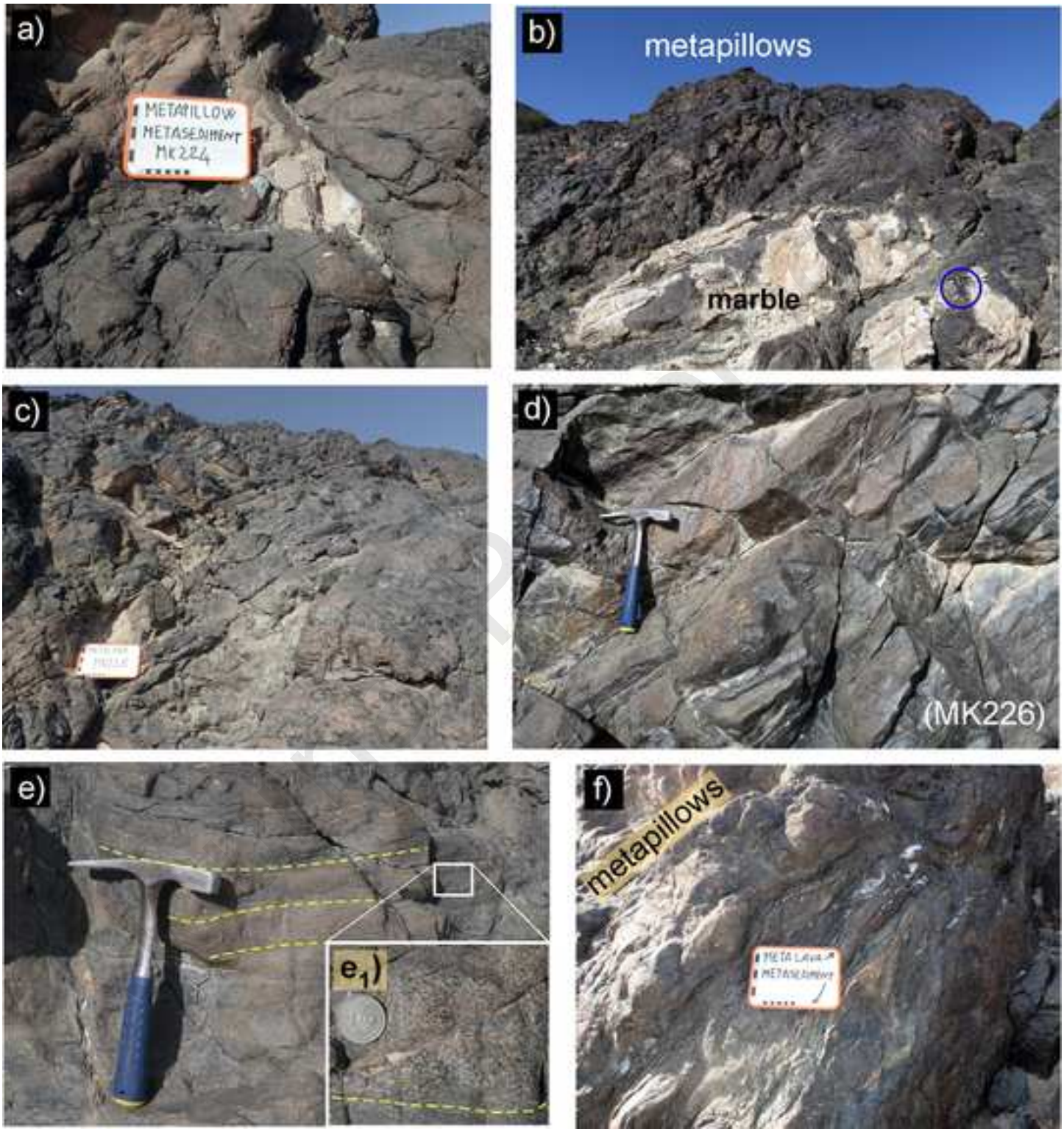
a)
METAPILLOW
METASEDIMENT
MK224
b)
metapillows
marble
c)
d)
(MK226)
e)
e1)
f)
metapillows

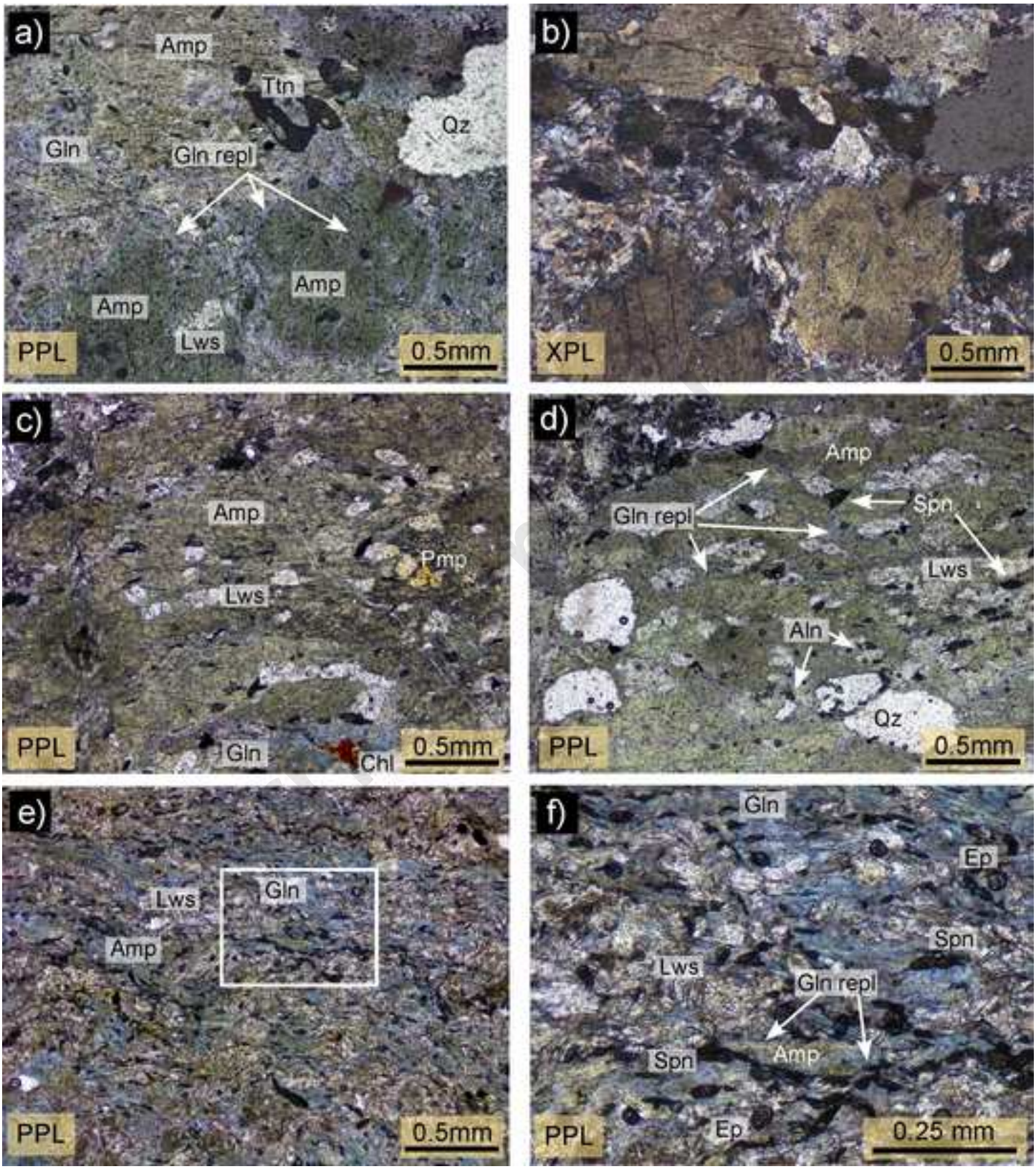

Figure 5 color for Online only

Click here to access/download;Figure;Fig_05.jpg

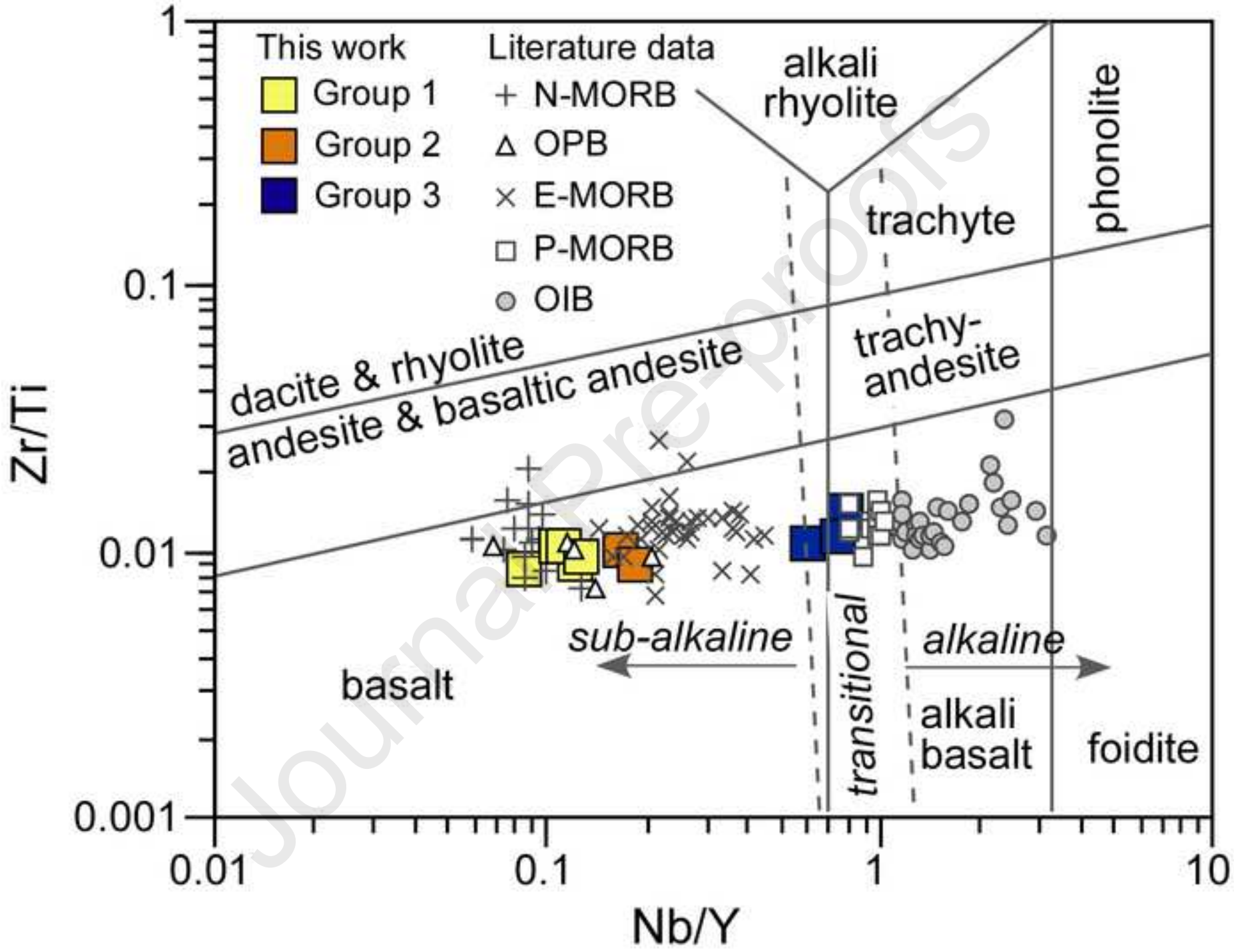

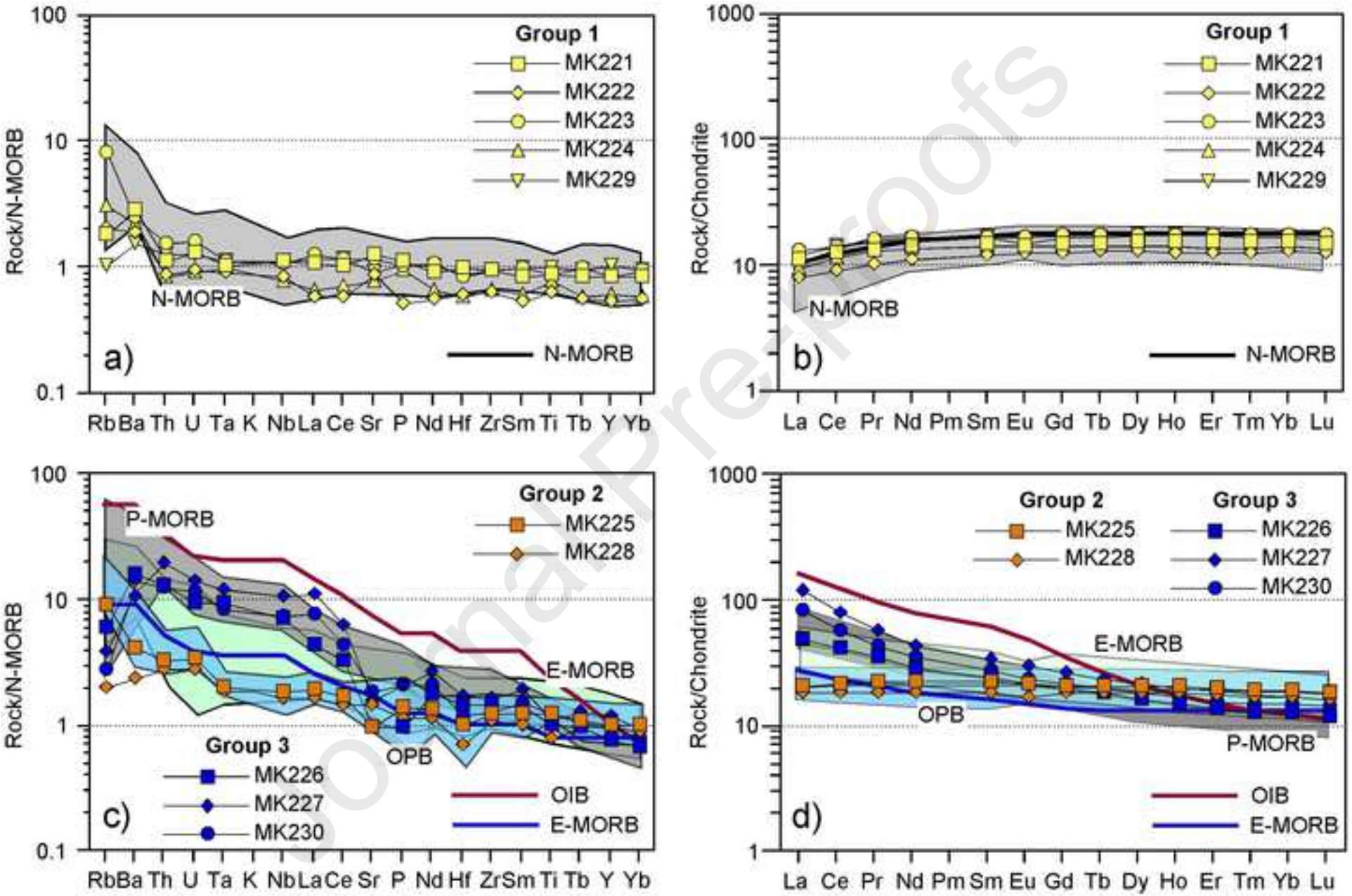

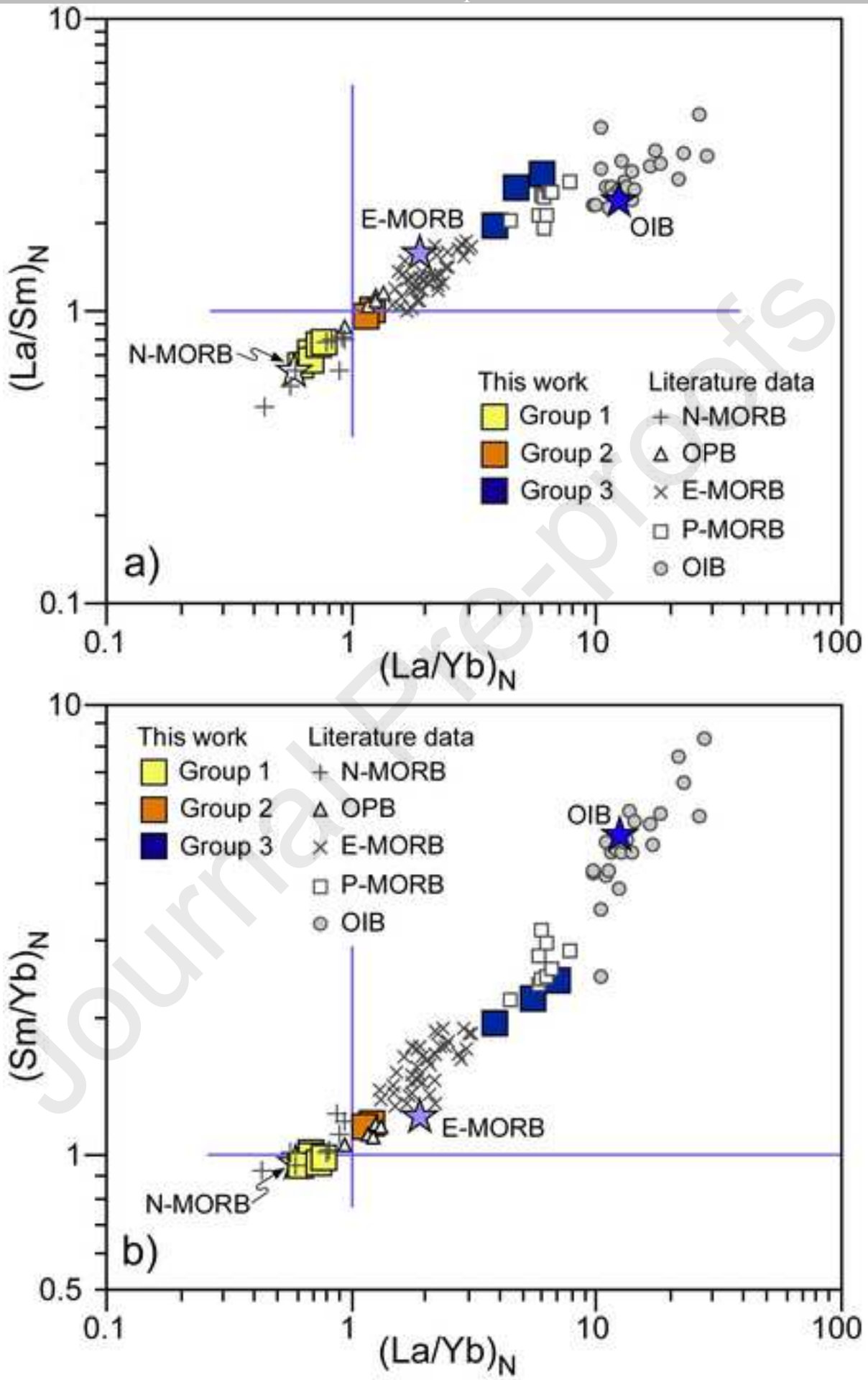

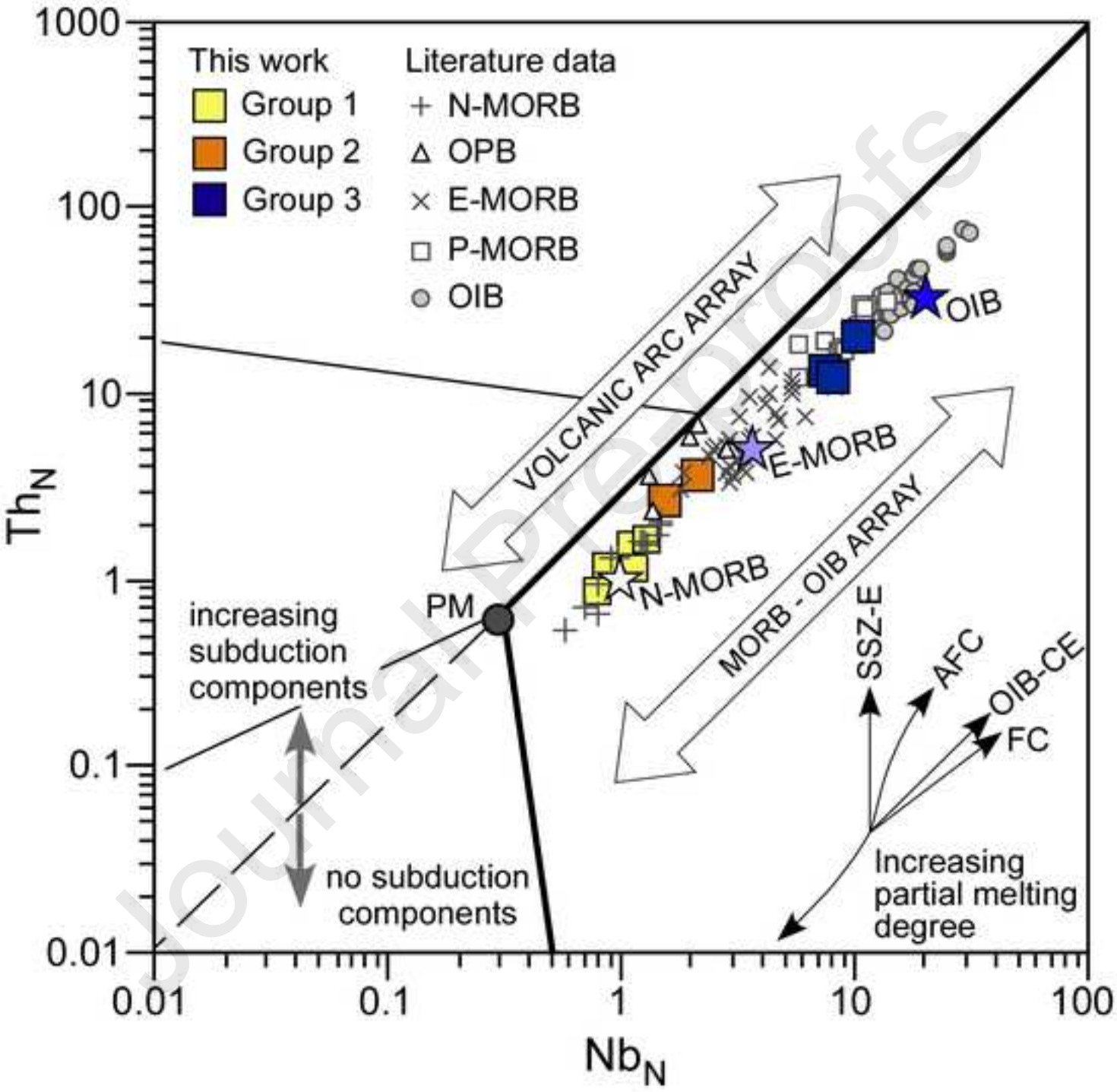

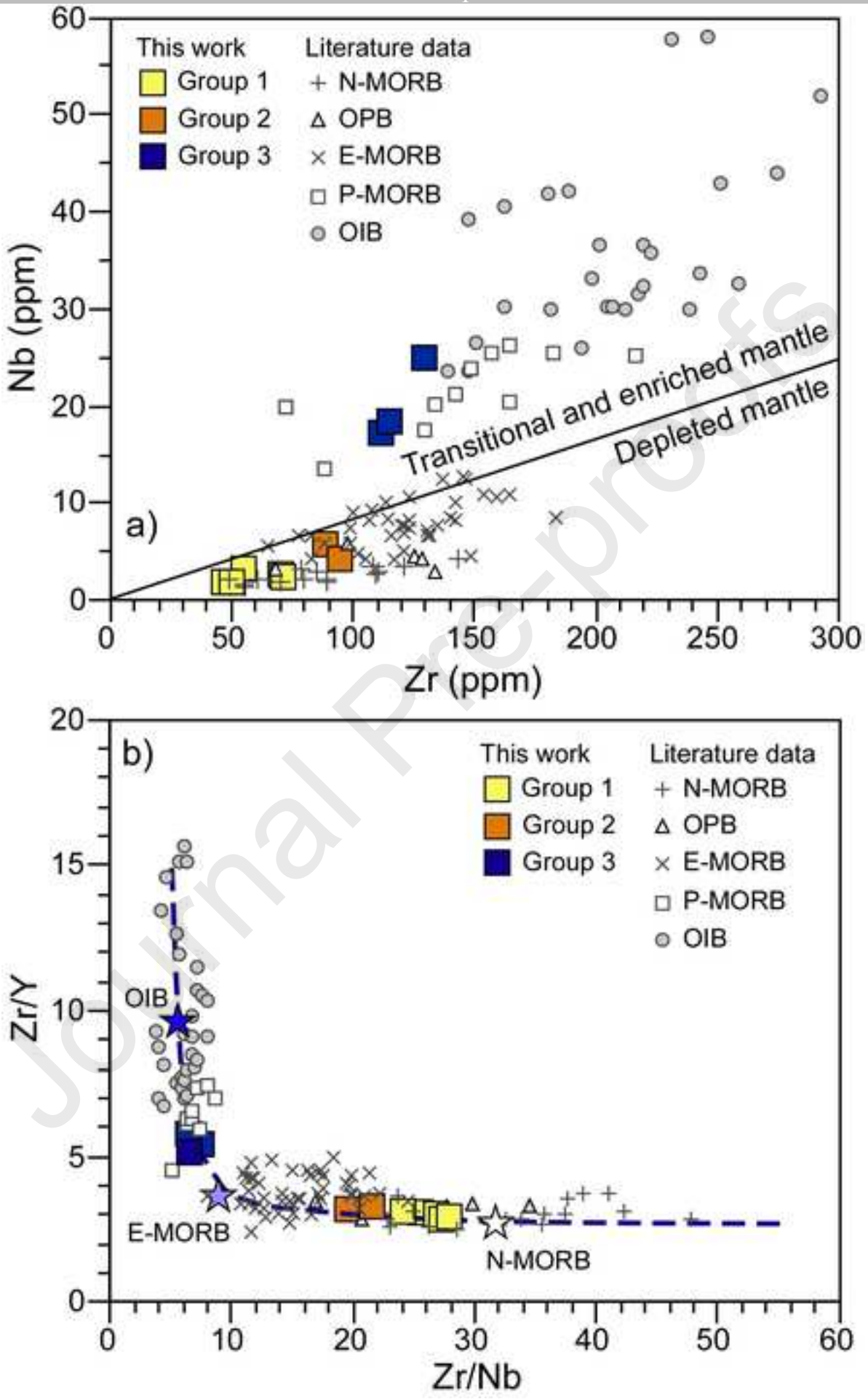

Figure 10 color for Online only

Click here to access/download;Figure;Fig_10.jpg

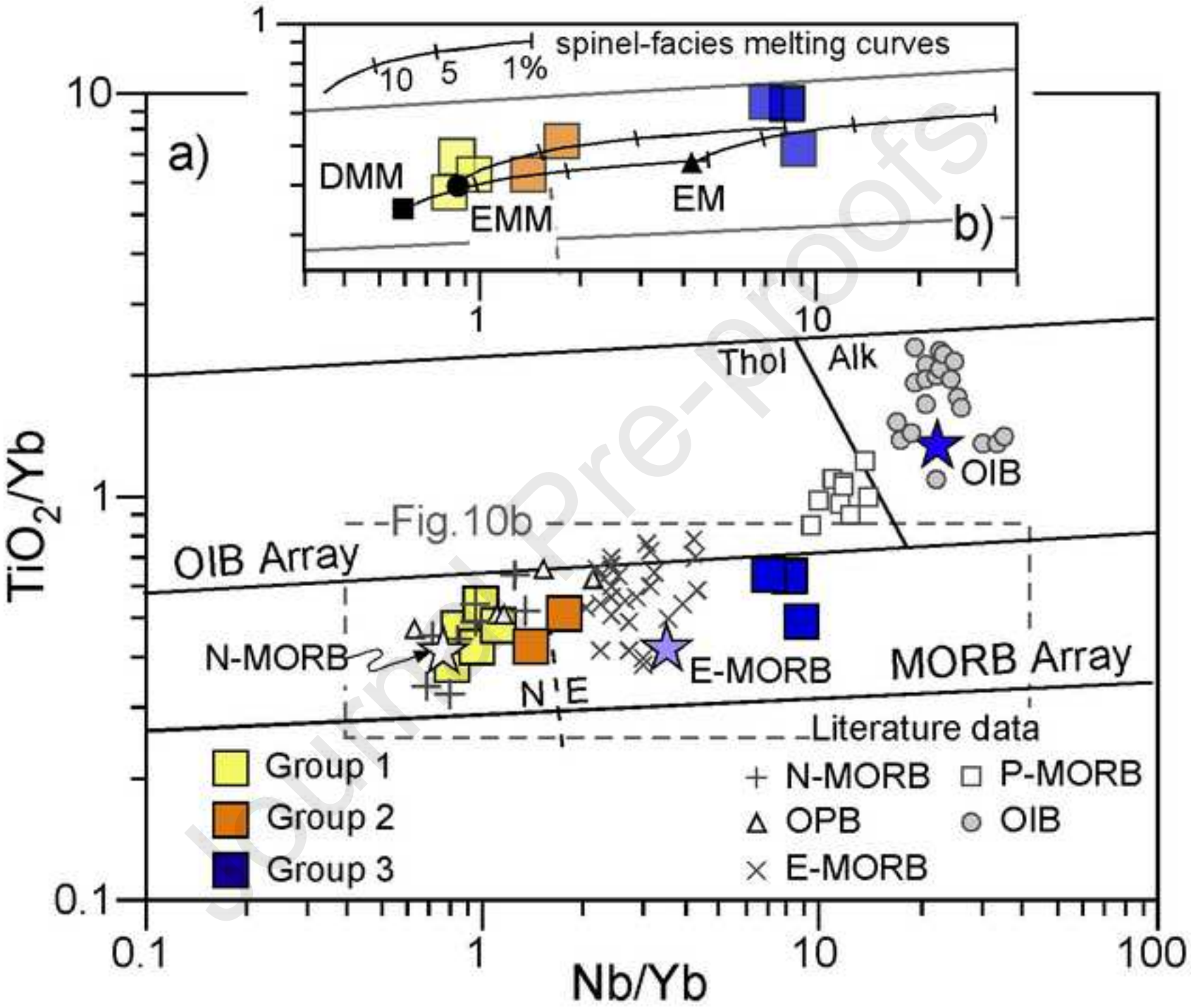

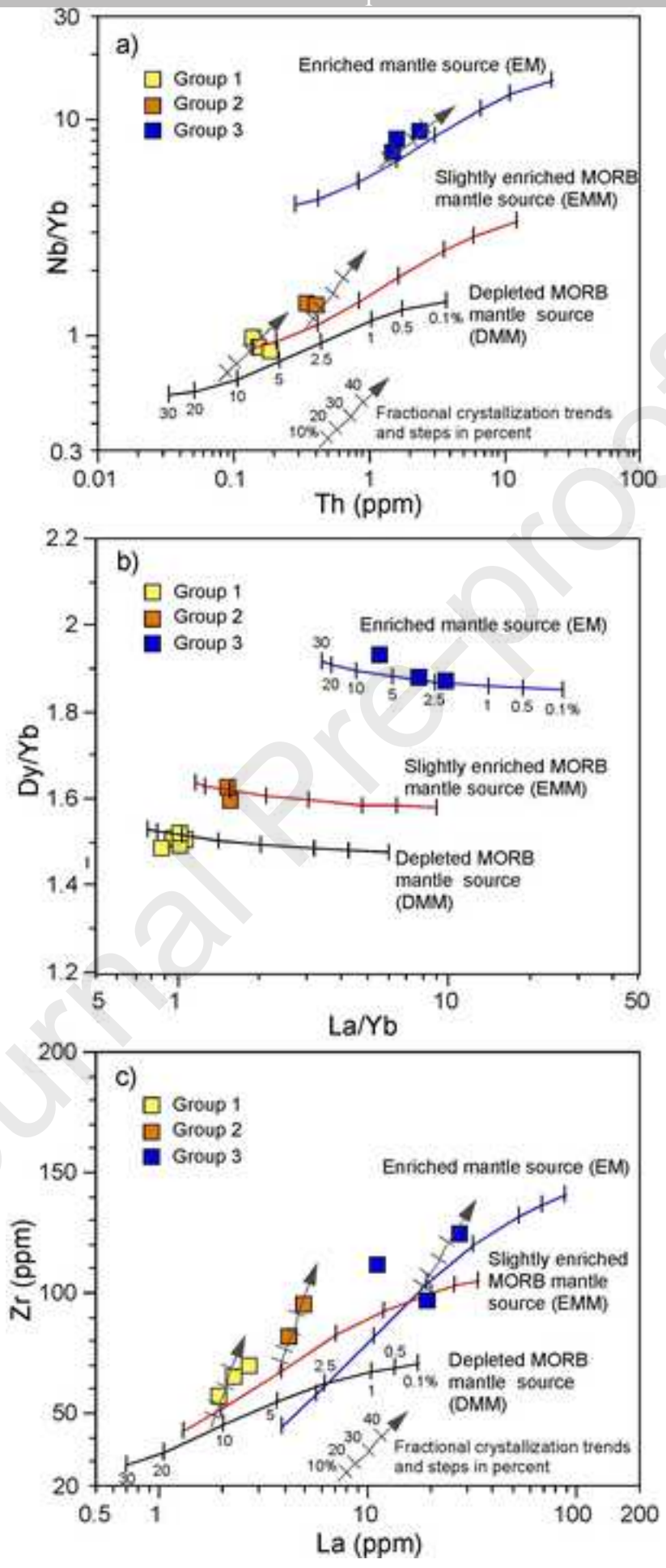

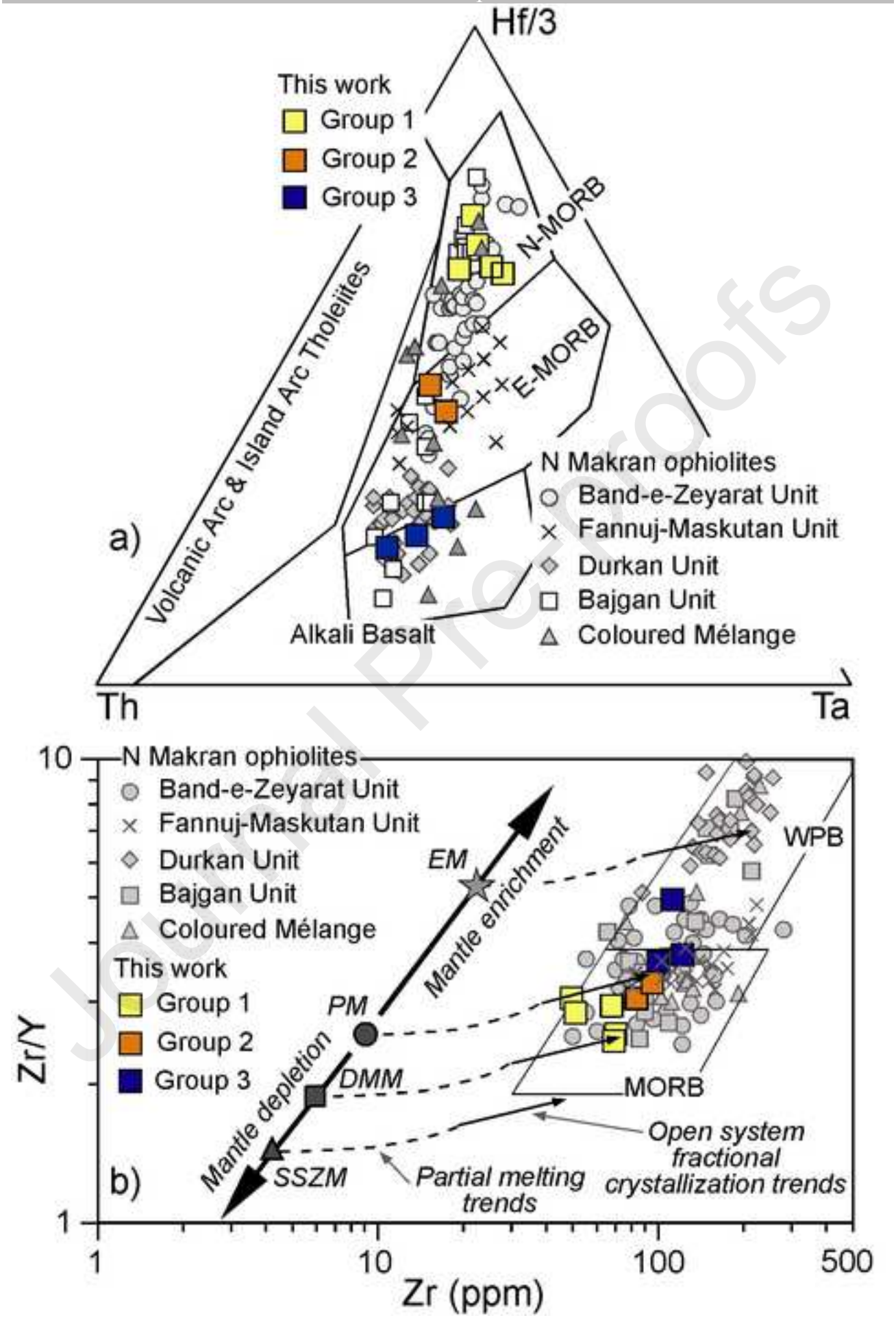

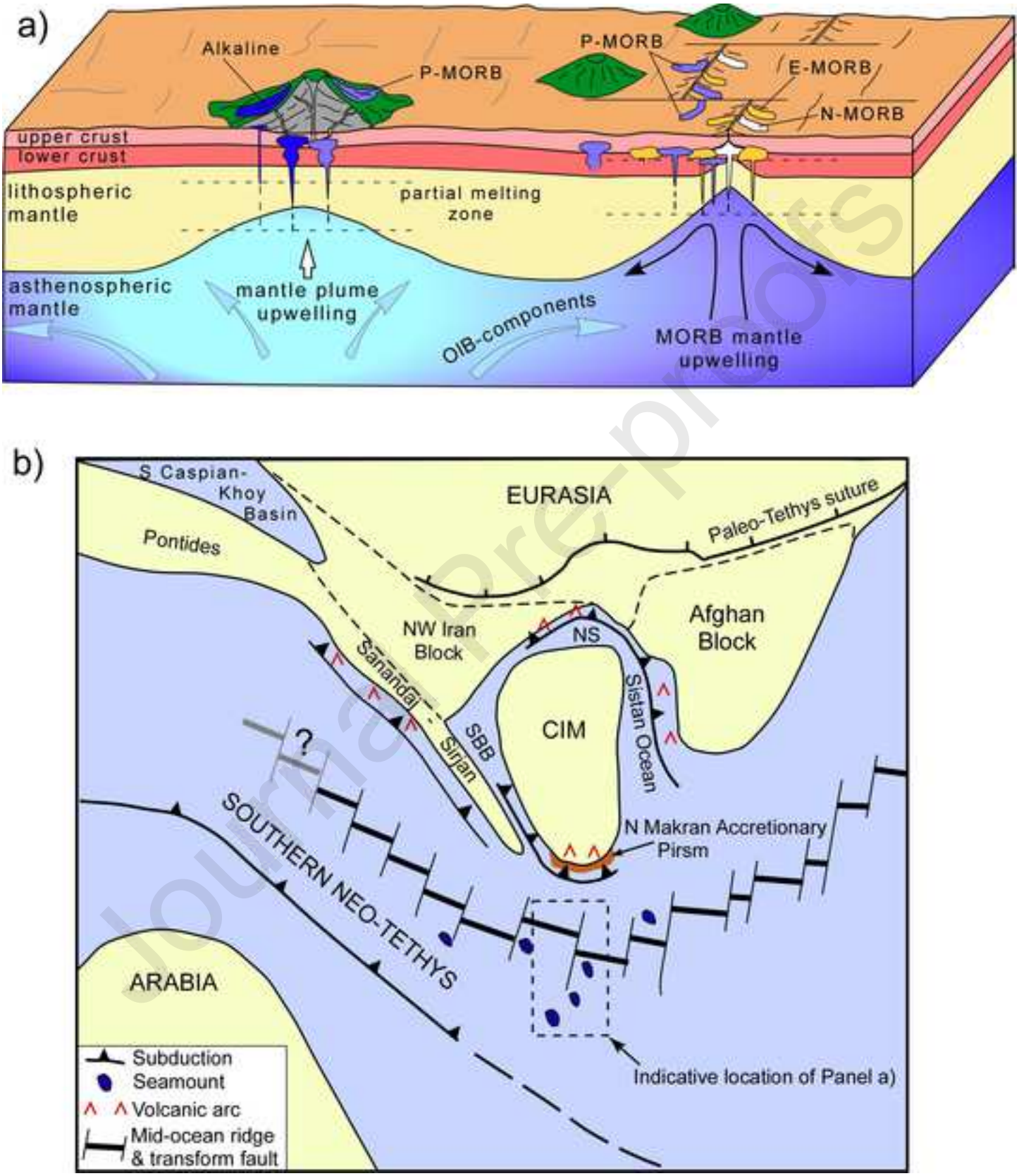

Figure 1 B&W for print only

Click here to access/download;Figure;Fig_01_BW.jpg

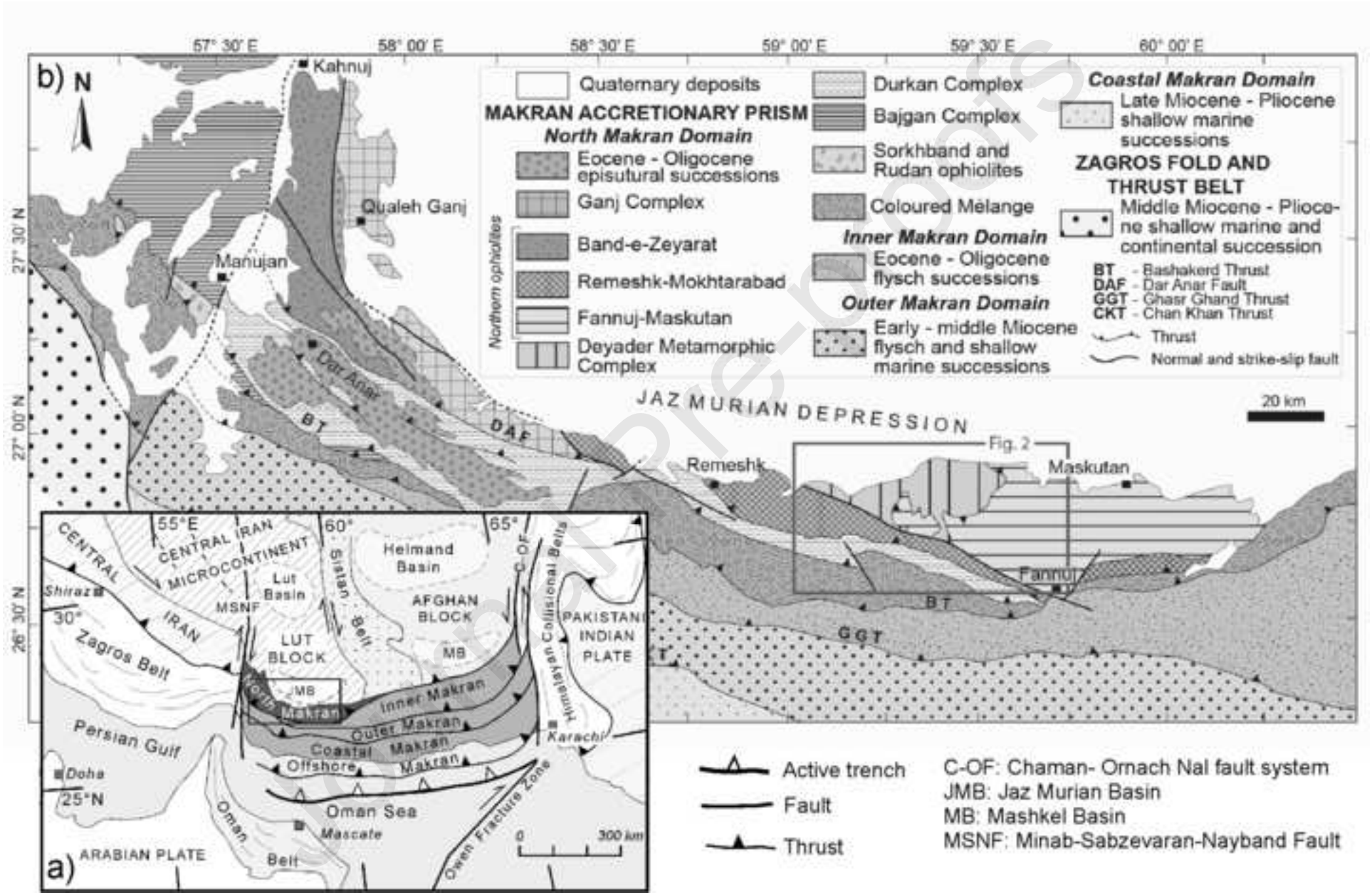

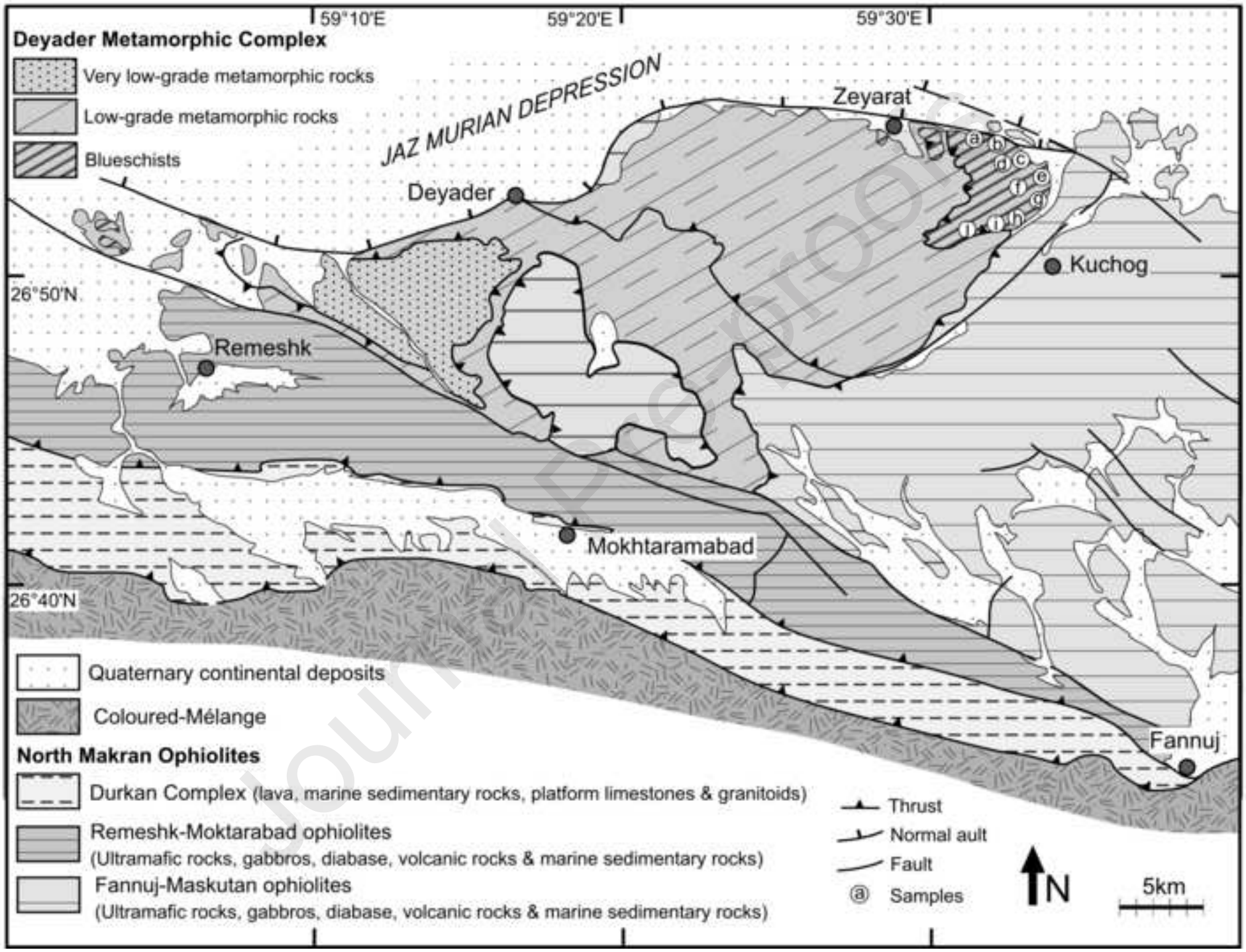

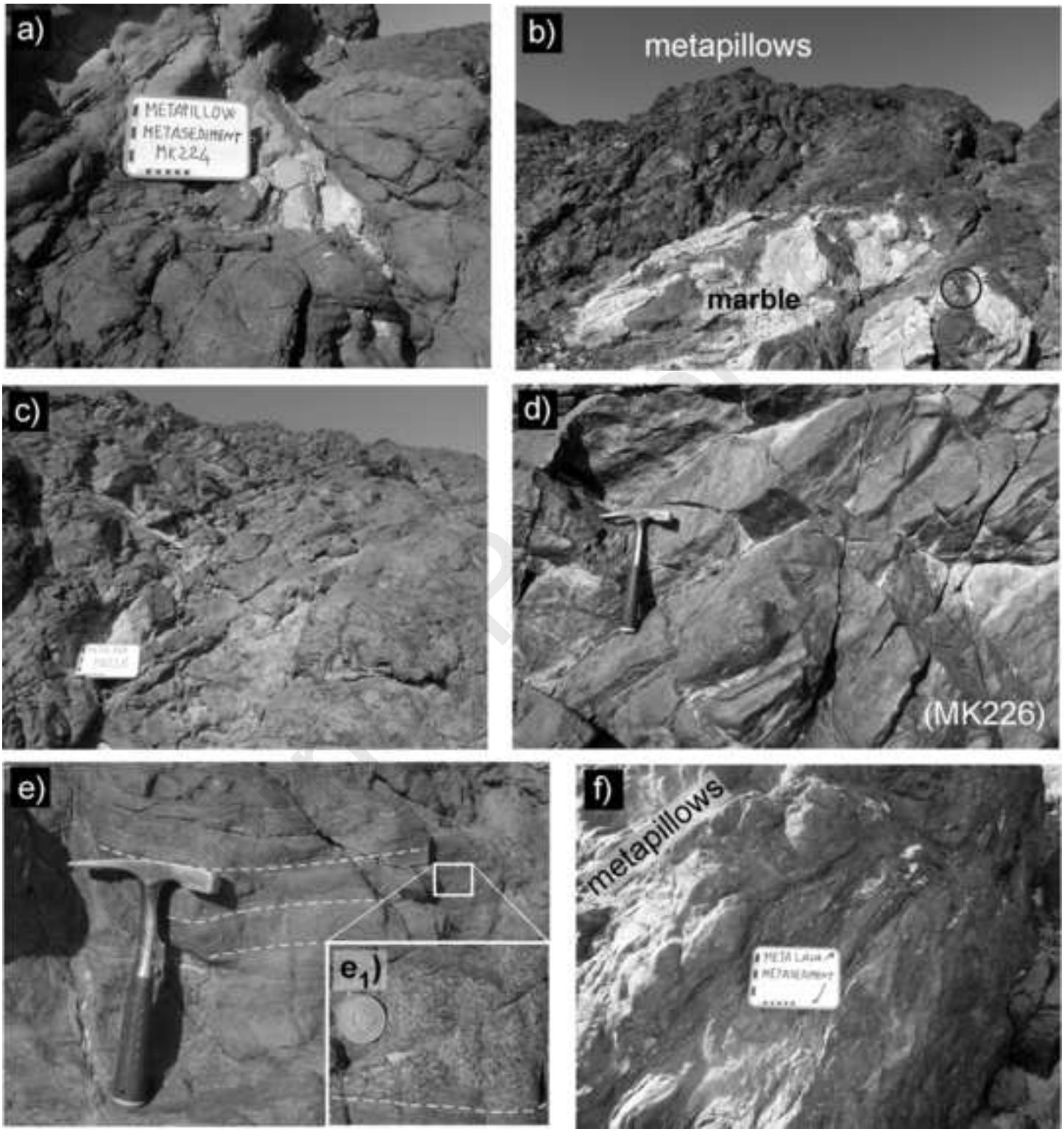
a)
METAPILLOW
METASEDIMENT
MK224
b)
metapillows
marble
c)
d)
(MK226)
e)
e1)
f)
metapillows

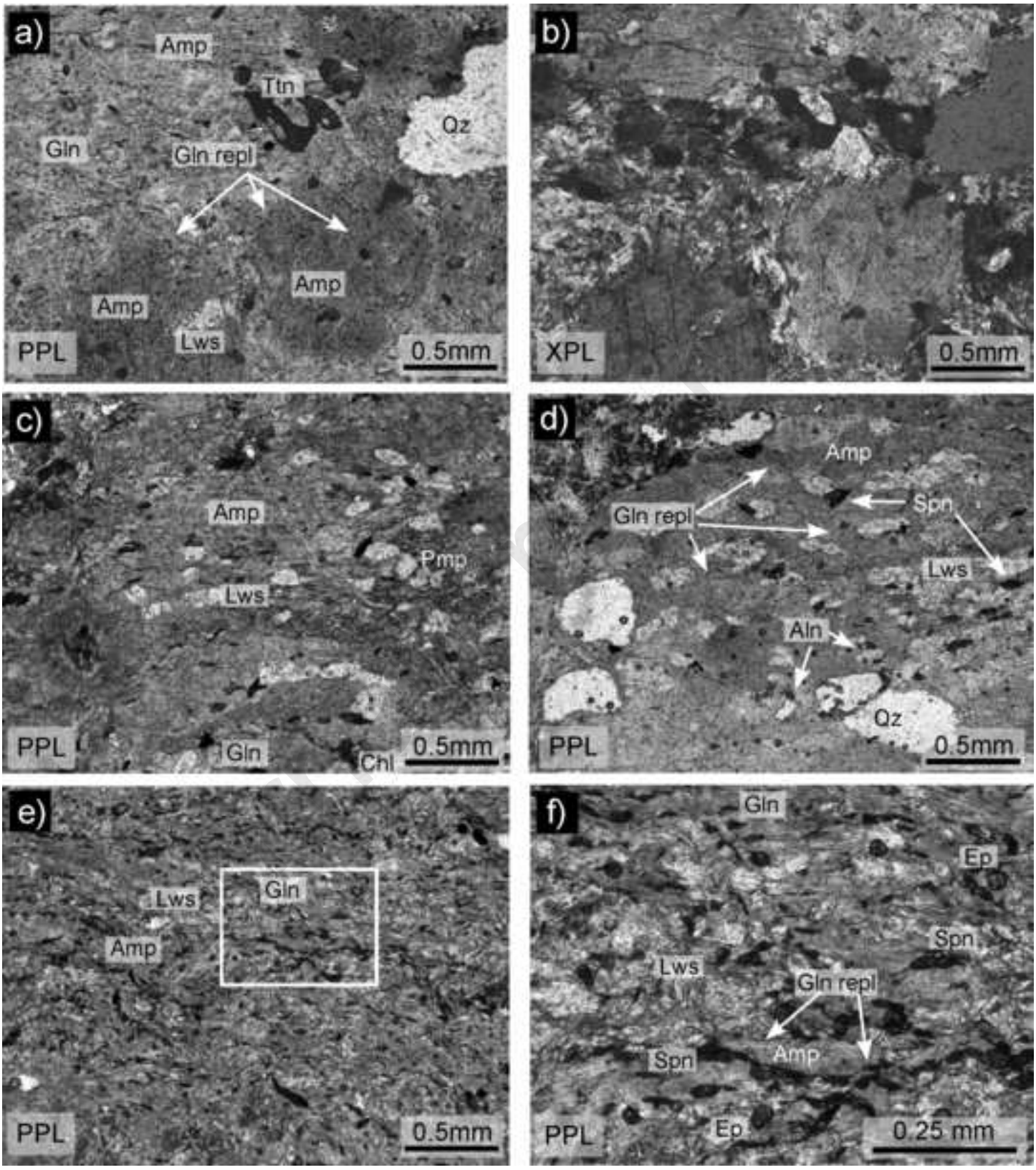

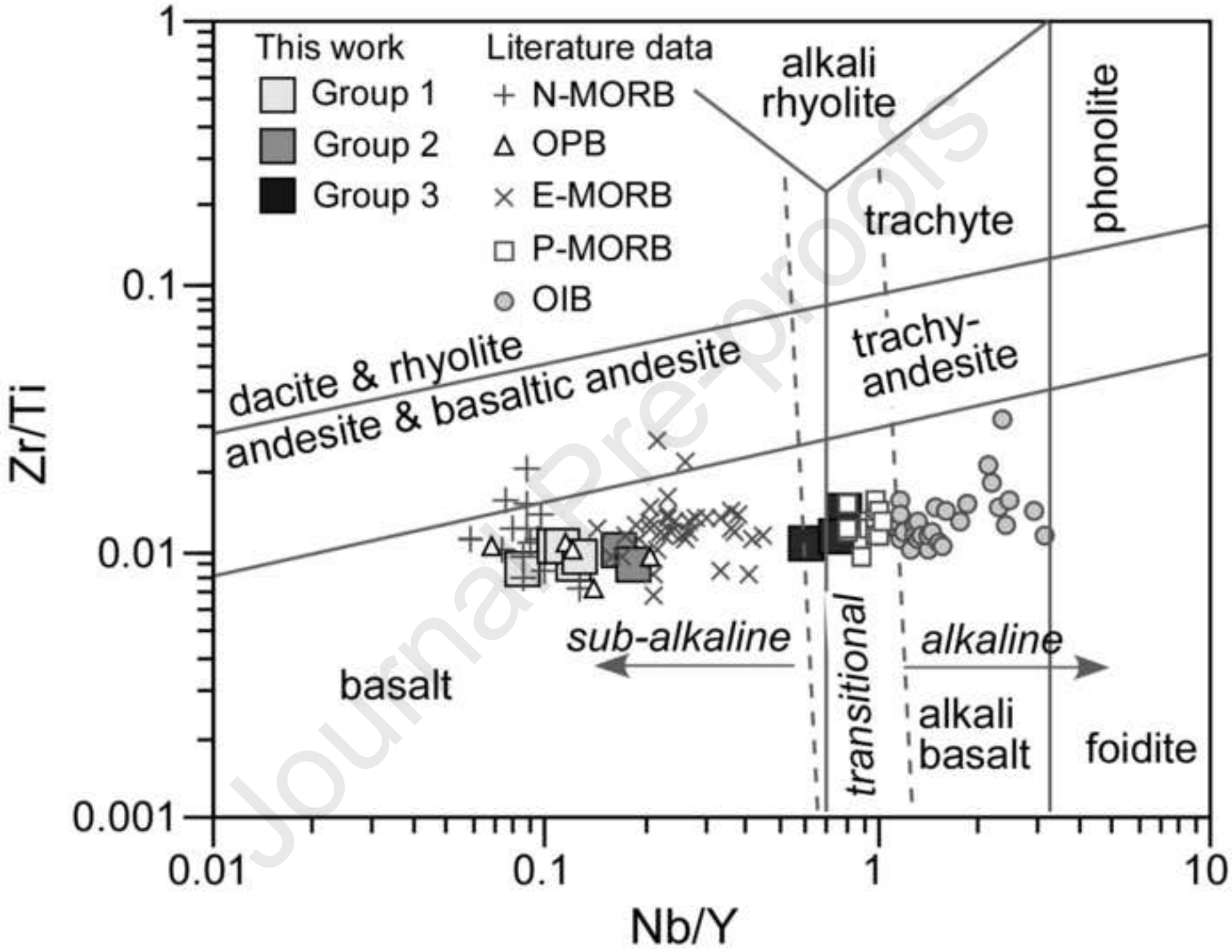

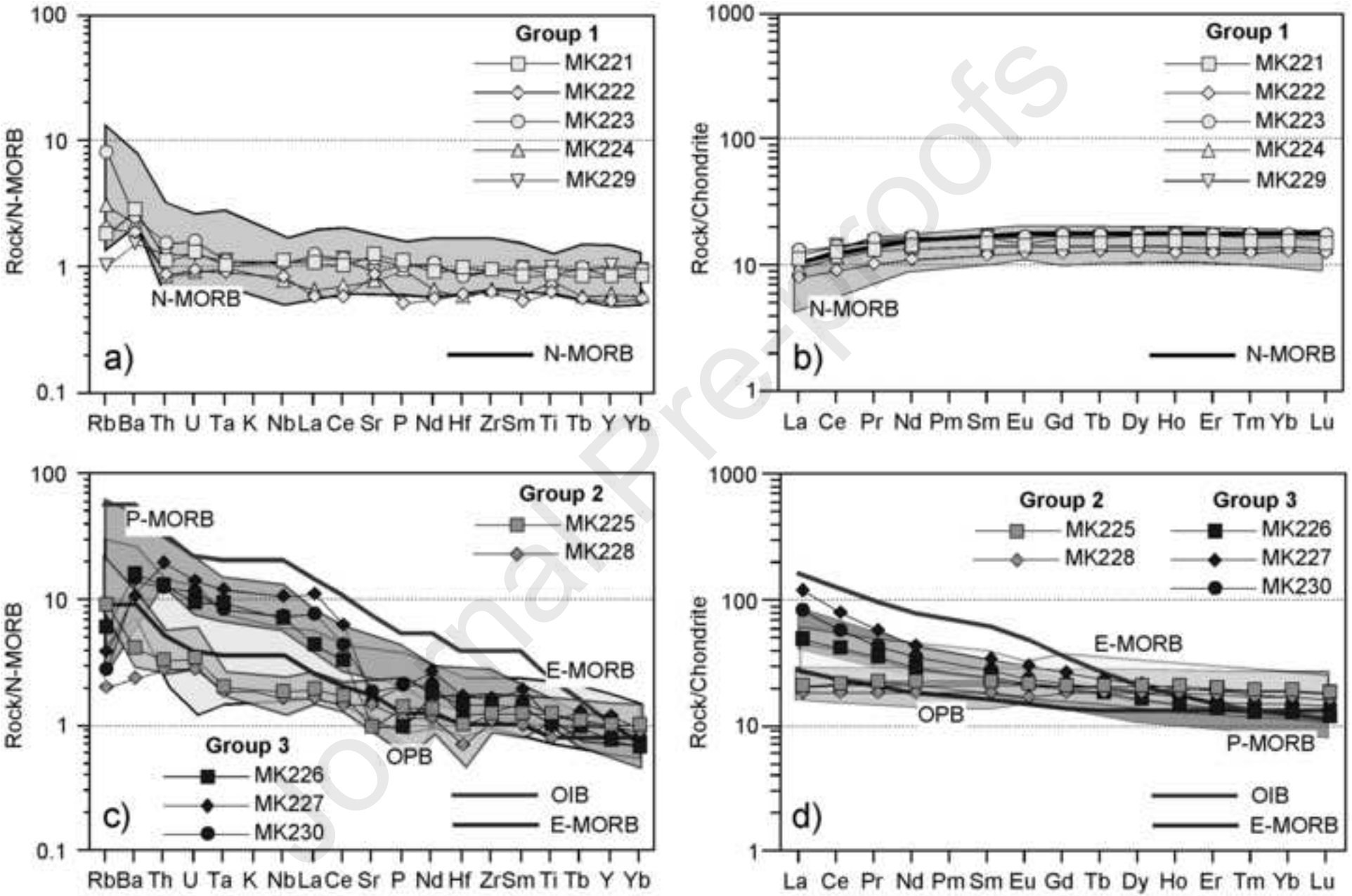

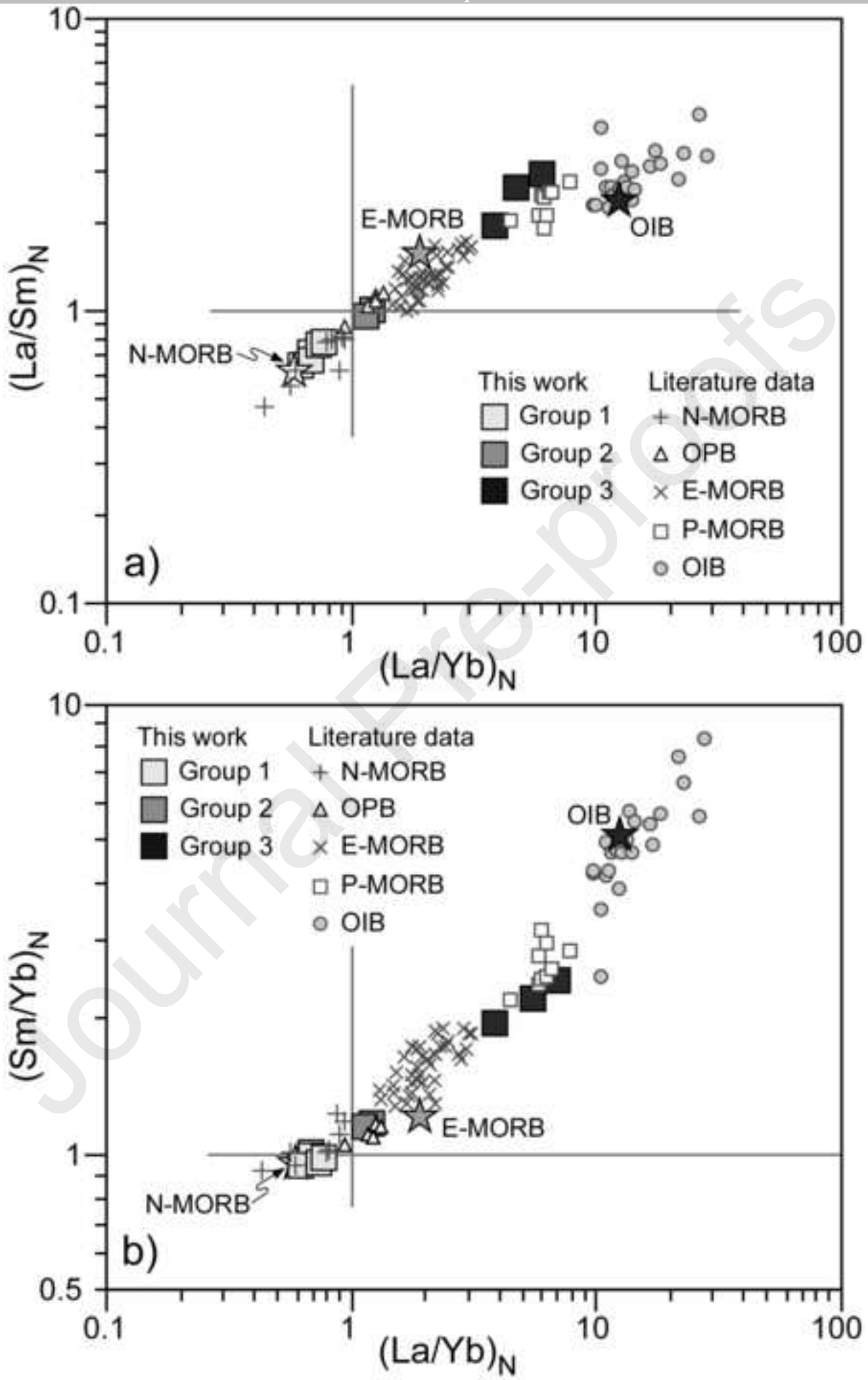

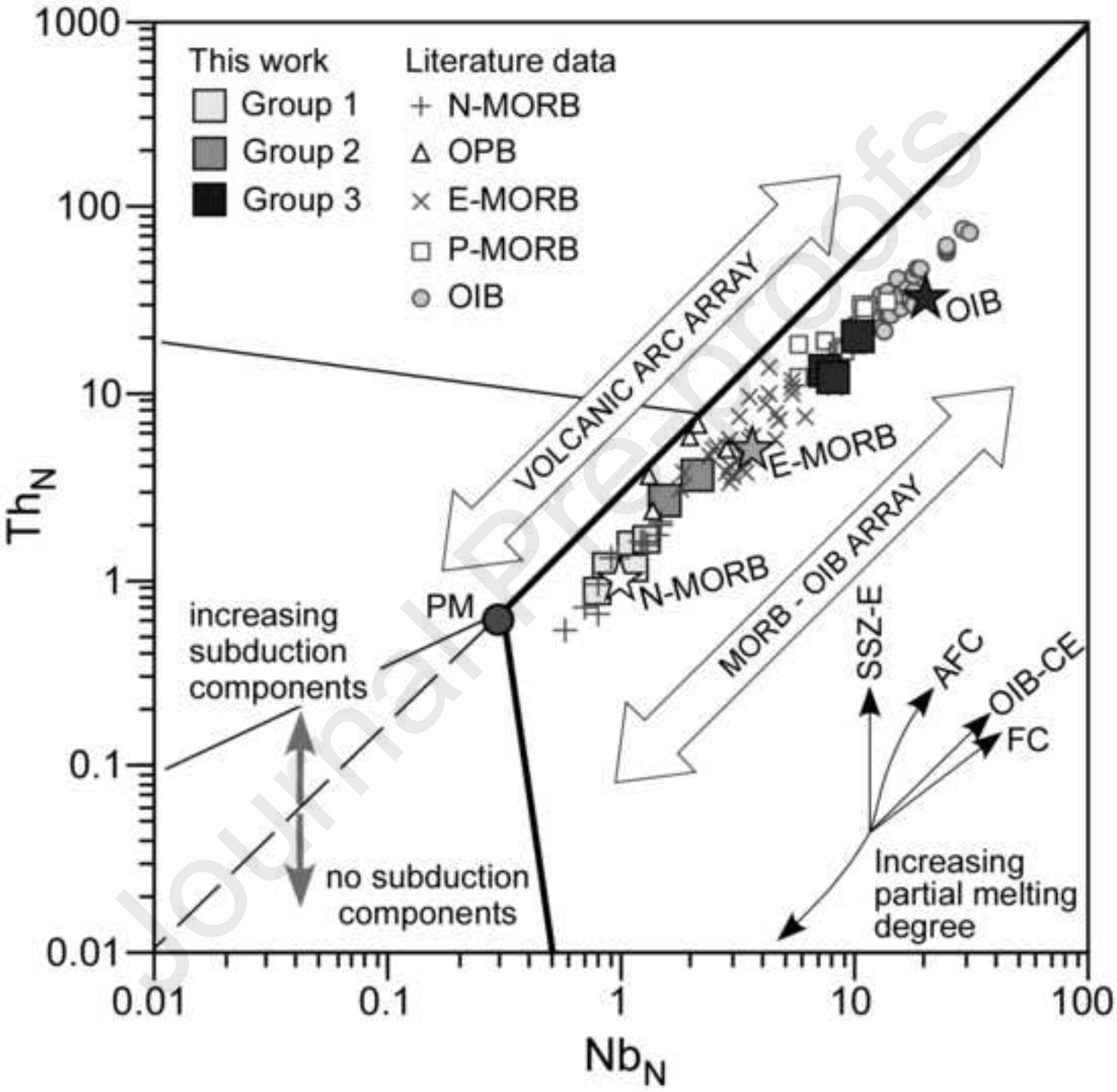

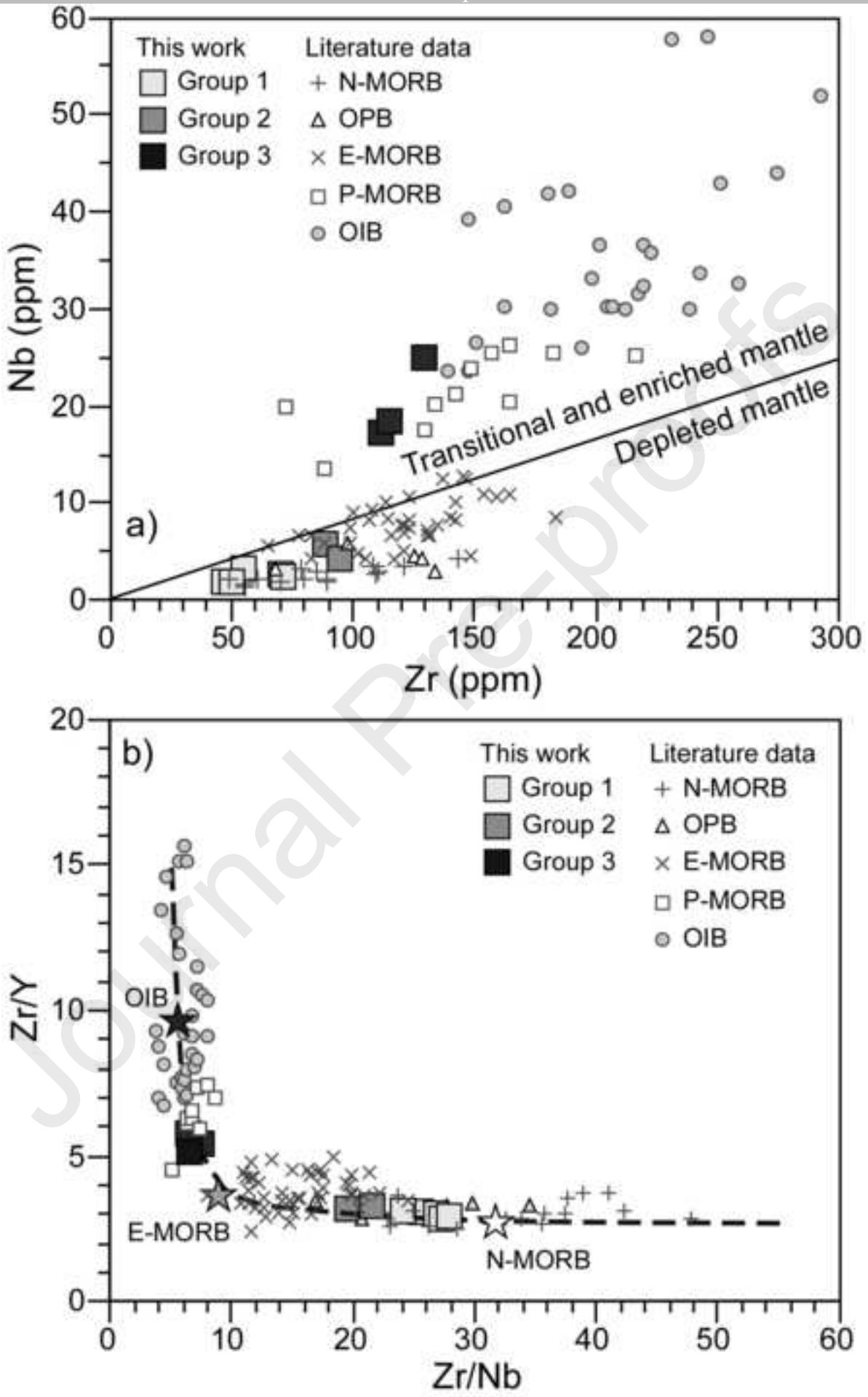

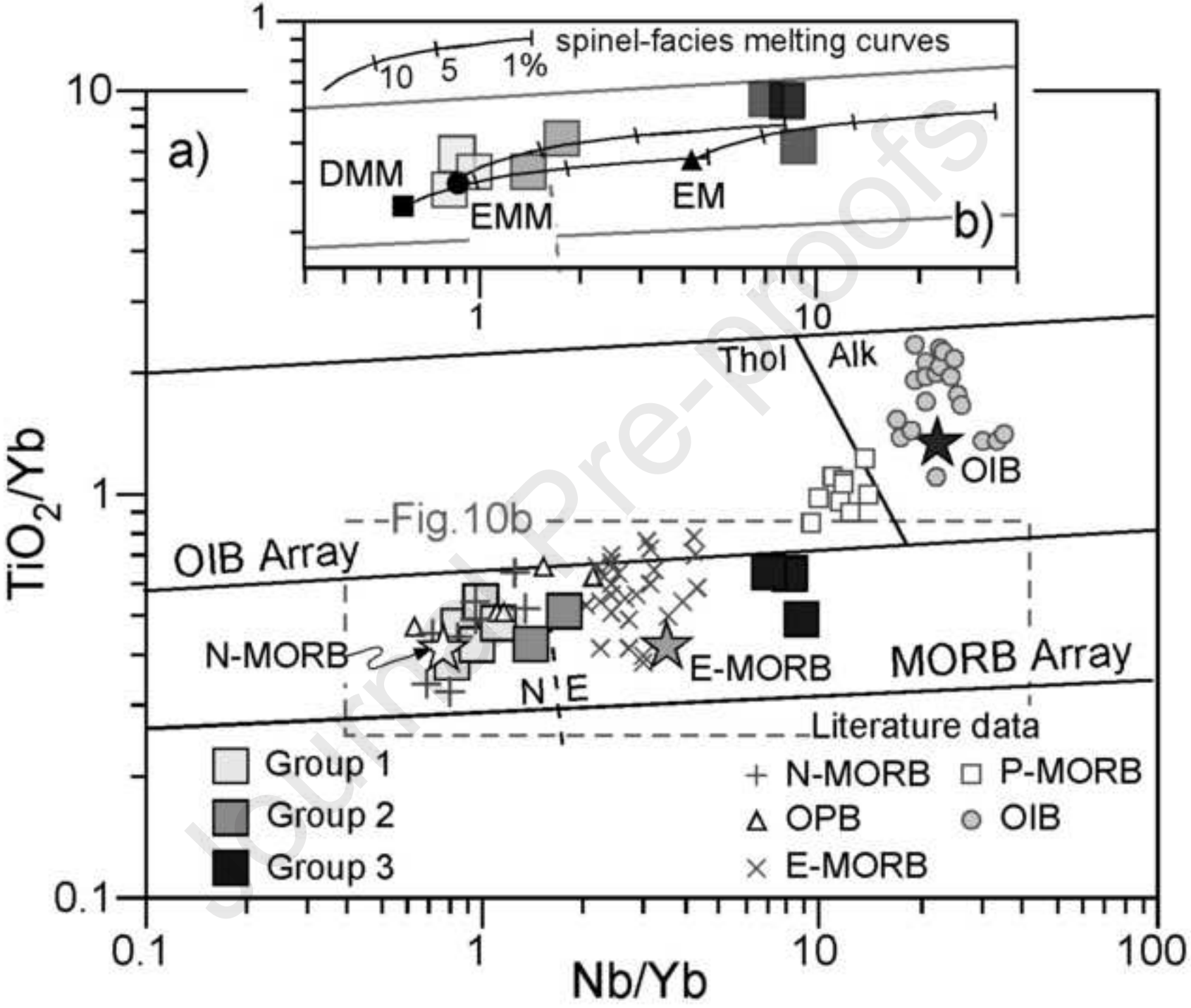

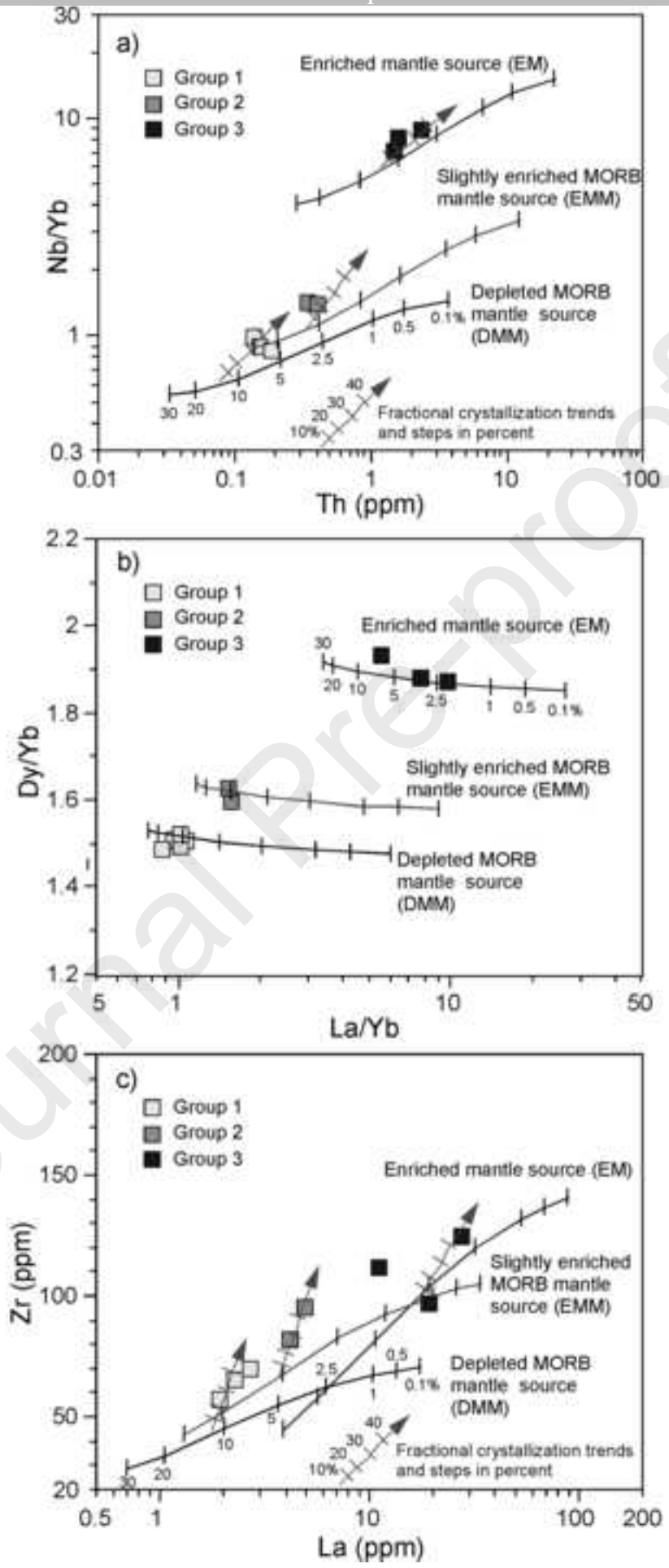

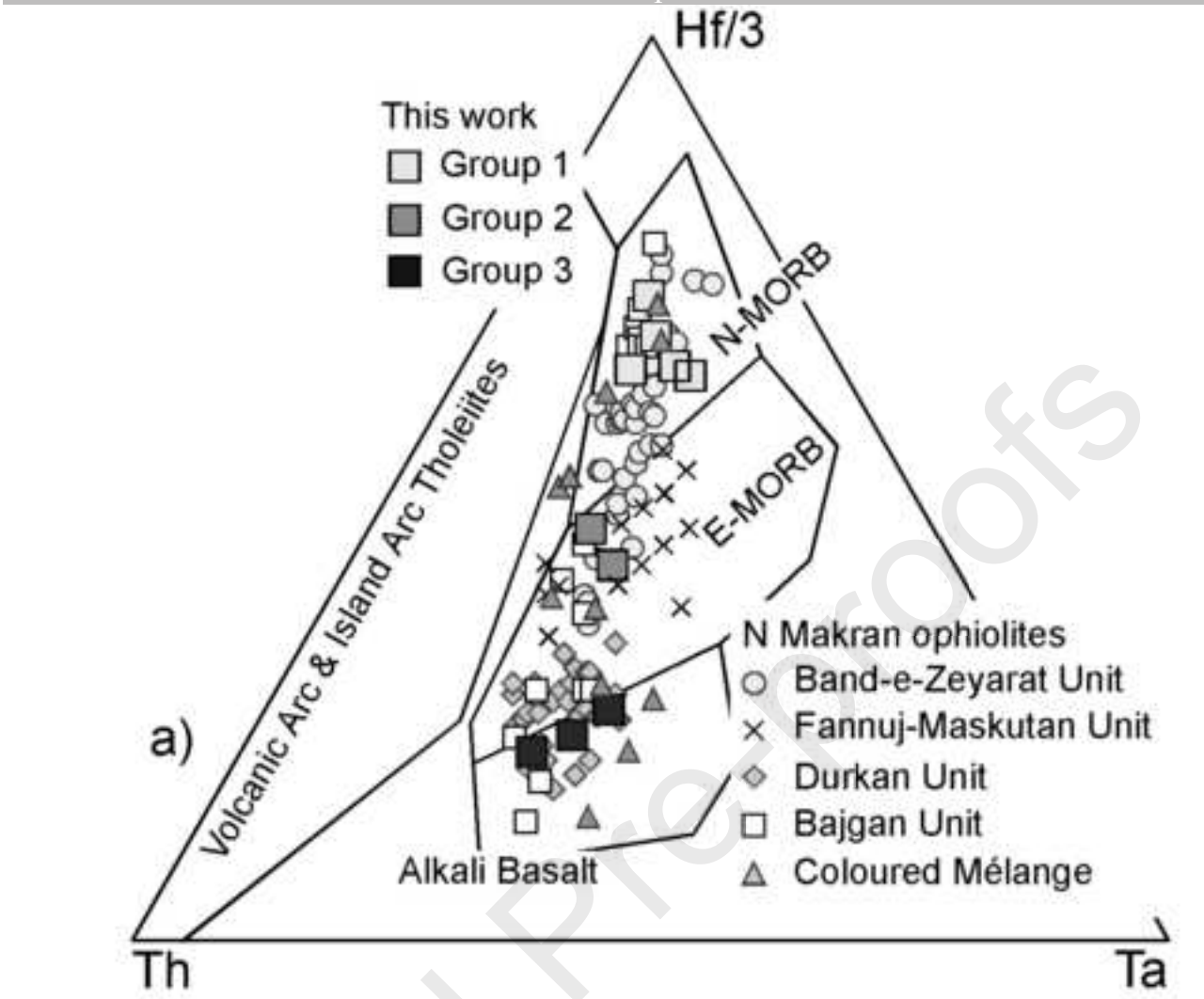

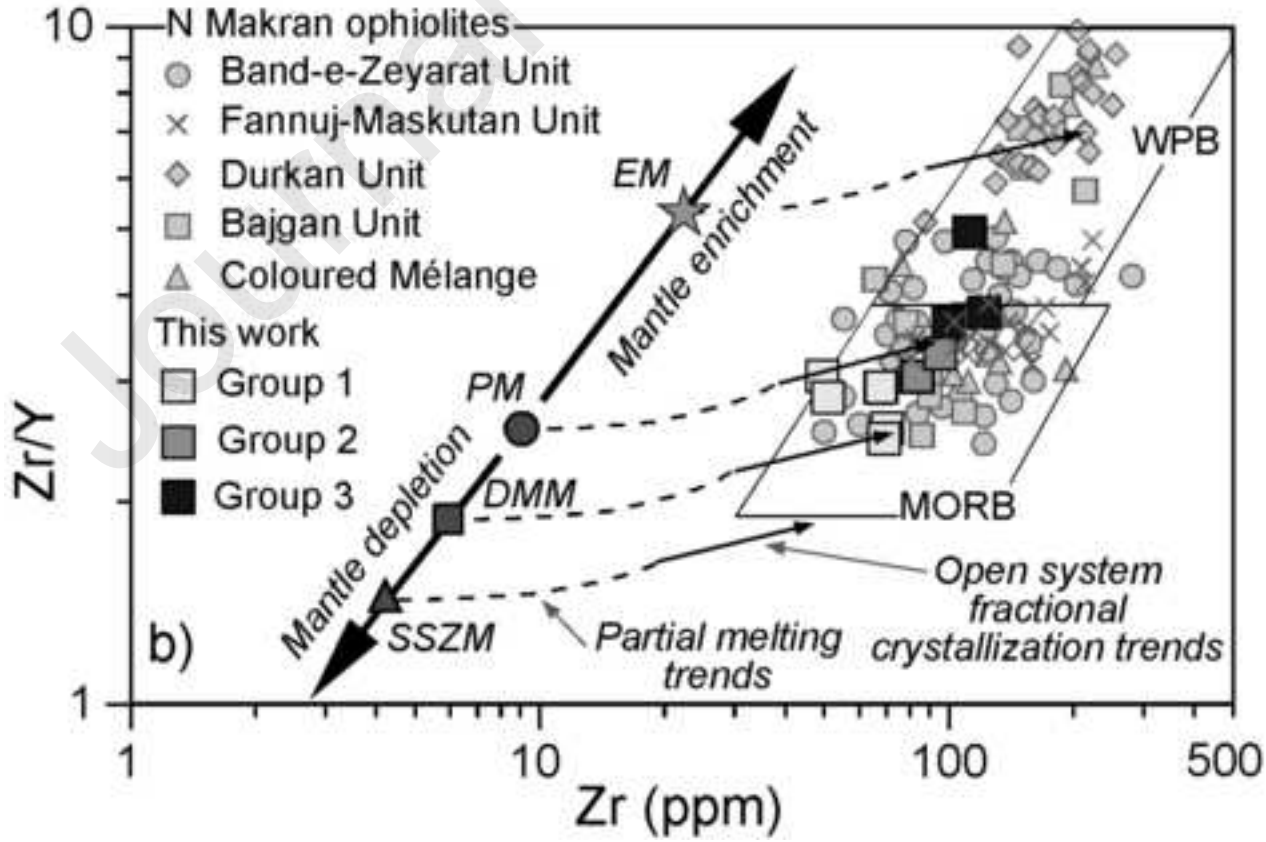

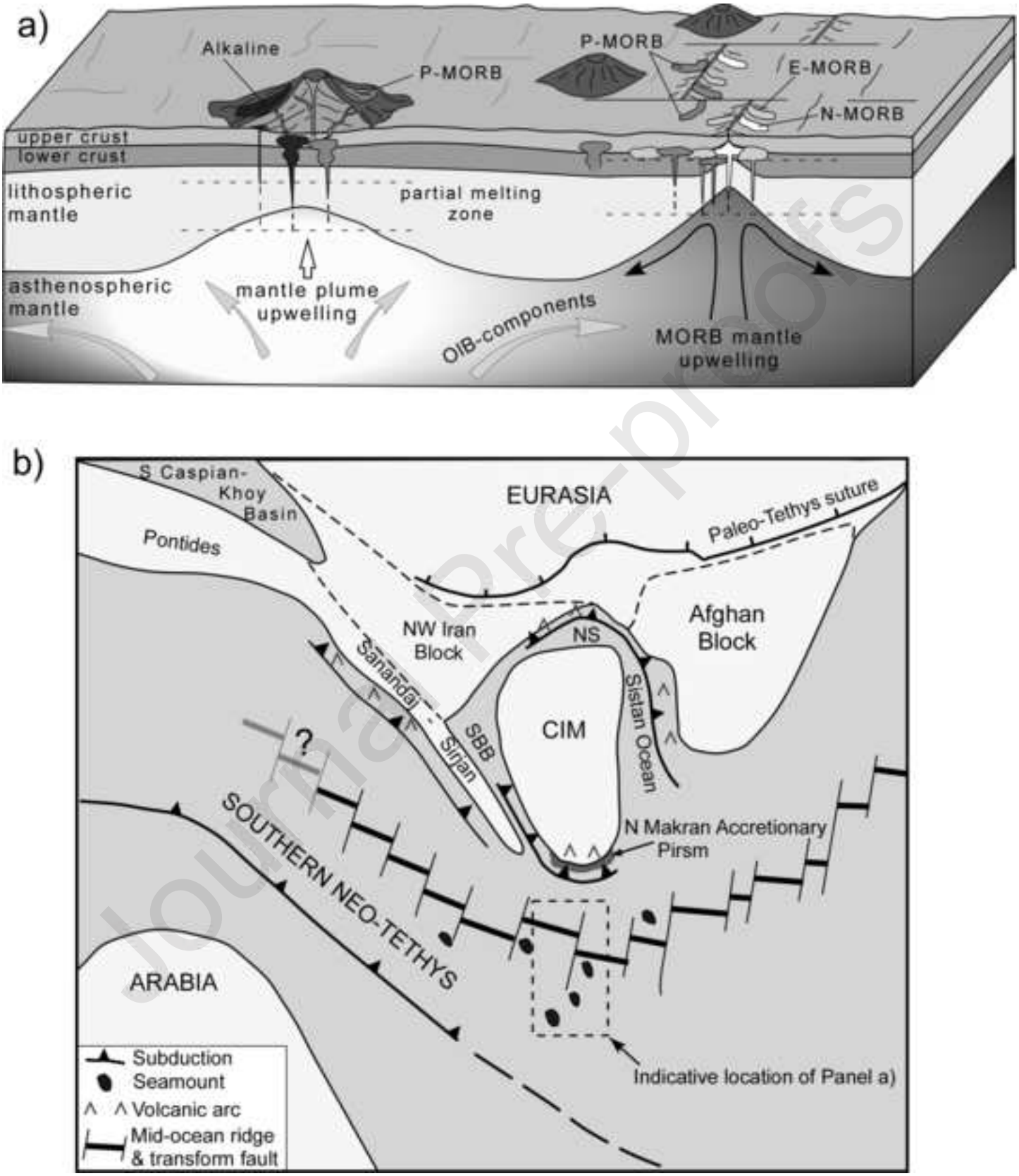

Rock Group	Group 1 (N-MORB)					Group 2 (E-MORB)		Group 3 (P-MORB)		
Sample	MK221	MK222	MK223	MK224	MK229	MK225	MK228	MK226	MK227	MK230
Field type	metapillow lavas	metapillow lavas	fine-grained massive basalt	metapillow lavas	fine-grained massive basalt	fine-grained massive basalt	fine-grained massive basalt	fine-grained massive basalt	fine-grained massive basalt	fine-grained massive basalt
Protolith	basalt	basalt	t	basalt	t	t	t	t	t	t
Sample location	a	b	c	d	i	e	h	f	g	j
XRF Analyses:										
SiO2	47.44	46.86	49.50	47.43	44.39	48.06	45.35	41.59	43.19	45.71
TiO2	1.09	0.79	1.10	0.93	1.21	1.53	0.99	1.25	1.32	1.52
Al2O3	15.68	14.97	14.88	14.57	12.34	14.05	13.19	14.51	12.35	13.51
Fe2O3	1.25	1.16	1.23	1.33	1.53	1.51	1.19	1.56	1.18	1.26
FeO	8.35	7.72	8.21	8.85	10.20	10.07	7.91	10.38	7.85	8.41
MnO	0.16	0.16	0.17	0.18	0.20	0.18	0.16	0.20	0.14	0.15
MgO	9.58	11.96	9.94	9.38	14.26	9.90	12.12	14.62	13.31	12.37
CaO	9.53	8.95	8.59	9.08	8.87	6.52	11.72	8.29	11.58	9.70
Na2O	2.95	2.44	2.27	3.19	2.92	3.05	3.01	1.78	2.58	2.44
K2O	0.14	0.15	0.52	0.24	0.12	0.33	0.13	0.23	0.17	0.19
P2O5	0.13	0.09	0.12	0.11	0.12	0.16	0.13	0.11	0.23	0.24
LOI	4.07	5.22	3.66	4.77	4.34	5.02	4.16	5.89	6.11	4.75
Total	100.36	100.48	100.20	100.06	100.52	100.37	100.06	100.39	100.01	100.25
Mg#	67.1	73.4	68.3	65.4	62.66	63.7	68.41	71.5	75.1	72.4
Zn	87	76	79	82	91	98	68	70	69	68
Cu	78	69	84	78	75	80	62	29	52	27
Sc	33	28	33	31	29	38	24	35	26	23
Ga	16	14	16	15	12	19	10	17	14	11
Ni	78	174	128	120	109	84	106	151	189	189
Co	40	41	40	40	66	40	61	41	65	80
Cr	404	460	367	415	271	289	362	431	366	334
V	277	202	251	253	317	302	273	307	282	356
Ba	18	20	18	14	10	43	25	88	72	83
Pb	11	10	11	11	7	14	6	10	7	7
ICP-MS Analyses:										
Rb	2.04	1.52	4.68	2.37	0.580	5.19	1.16	3.38	2.24	1.57
Sr	116	104	108	96.8	82.1	88.0	133	87.7	147	170
	23.6	20.1	24.0	23.8	29.2	29.0	27.23	21.96	33.5	27.6
Zr	70.2	56.9	70.9	64.9	72.0	95.0	81.37	112	124	97.0
Nb	2.62	2.56	2.54	2.47	2.61	4.42	3.98	17.2	25.1	17.6
La	2.69	1.93	3.18	2.30	2.94	4.90	4.19	11.2	27.8	19.4
Ce	7.78	5.72	8.97	7.20	8.95	12.9	10.96	25.0	47.6	33.8
Pr	1.29	0.981	1.53	1.25	1.49	2.05	1.71	3.25	5.22	4.06
Nd	6.73	5.35	7.83	6.56	7.71	10.1	8.47	13.3	19.8	15.9
Sm	2.27	1.89	2.65	2.21	2.59	3.30	2.76	3.67	5.13	4.09
Eu	0.854	0.743	1.00	0.832	0.861	1.22	0.970	1.25	1.70	1.35

Gd	3.16	2.66	3.63	2.97	3.51	4.20	3.66	4.06	5.27	4.32
Tb	0.569	0.493	0.660	0.535	0.639	0.757	0.670	0.666	0.863	0.724
Dy	3.94	3.32	4.50	3.64	4.44	5.05	4.53	4.04	5.30	4.59
Ho	0.882	0.732	1.00	0.807	1.00	1.13	1.01	0.845	1.08	0.929
Er	2.59	2.14	2.88	2.34	2.90	3.24	2.85	2.25	3.03	2.57
Tm	0.400	0.332	0.453	0.358	0.442	0.486	0.429	0.321	0.433	0.373
Yb	2.63	2.24	2.98	2.41	2.92	3.16	2.78	2.08	2.84	2.46
Lu	0.385	0.331	0.442	0.360	0.423	0.464	0.409	0.292	0.399	0.359
Hf	2.08	1.62	1.74	1.66	1.80	2.13	1.48	2.99	3.60	2.52
Ta	0.136	0.160	0.149	0.176	0.147	0.272	0.248	1.28	1.59	1.11
Th	0.138	0.137	0.185	0.136	0.153	0.407	0.346	1.58	2.35	1.51
U	0.062	0.058	0.076	0.058	0.060	0.164	0.133	0.460	0.691	0.558
Nb/Y	0.11	0.13	0.11	0.10	0.09	0.15	0.15	0.78	0.75	0.64
Ti/V	24	25	27	23	24	32	23	26	30	27
Nb/Yb	1.00	1.15	0.85	1.03	0.89	1.40	1.43	8.23	8.85	7.15
Th/Ta	1.02	0.86	1.24	0.77	1.04	1.50	1.39	1.23	1.48	1.35
Th/Tb	0.24	0.28	0.28	0.25	0.24	0.54	0.52	2.38	2.73	2.08
(La/Sm)N	0.76	0.66	0.78	0.67	0.73	0.96	0.98	1.96	3.49	3.07
(Sm/Yb)N	0.96	0.94	0.99	1.02	0.99	1.16	1.10	1.96	2.01	1.85
(La/Yb)N	0.73	0.62	0.77	0.68	0.72	1.11	1.08	3.85	7.02	5.68

Highlights

- The Deyader Complex in the Makran includes a blueschist HT-LP metaophiolitic unit
- Blueschist volcanic protoliths show N-MORB, E-MORB, and P-MORB affinities
- Volcanic protoliths were erupted in mid-ocean ridge featuring plume-ridge interaction
- Blueschists show geochemical features similar to those of the Makran ophiolites

Tectono-magmatic settings of formation and composition of the volcanic protoliths of the Blueschist Unit from the Deyader Complex (Makran Accretionary Prism, SE Iran)

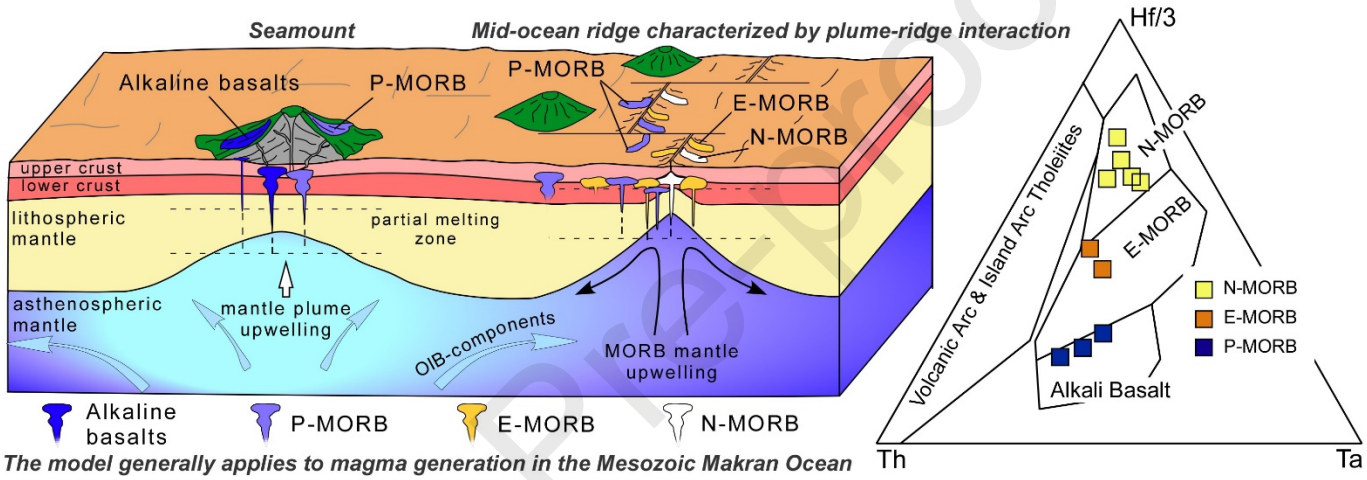

The model generally applies to magma generation in the Mesozoic Makran Ocean

Title: Geochemistry of basaltic blueschists from the Deyader Metamorphic Complex (Makran Accretionary Prism, SE Iran): New constraints for magma generation in the Makran sector of the Neo-Tethys.

Geochemistry (Chemie der Erde)

CRediT author statement

Emilio Saccani: Conceptualization, Investigation, Writing - Review & Editing, Project administration, Funding acquisition. **Morteza Delavari:** Conceptualization, Investigation, Writing - Review & Editing. **Asghar Dolati:** Conceptualization, Investigation, Writing - Review & Editing. **Luca Pandolfi:** Conceptualization, Investigation, Writing - Review & Editing, Project administration. **Edoardo Barbero:** Conceptualization, Investigation, Writing - Original Draft, Writing - Review & Editing. **Renzo Tassinari:** Investigation, Formal analysis. **Michele Marroni:** Conceptualization, Investigation, Writing - Review & Editing, Project administration, Funding acquisition.

Declaration of interests

☒ The authors declare that they have no known competing financial interests or personal relationships that could have appeared to influence the work reported in this paper.

☐The authors declare the following financial interests/personal relationships which may be considered as potential competing interests: